Fall 2016

FABRICATION AND CHARACTERIZATION OF CONDUCTIVE MELT ELECTROSPUN FIBERS

Brandon Ross
Montana Tech

FABRICATION AND CHARACTERIZATION OF CONDUCTIVE MELT ELECTROSPUN FIBERS

by

Brandon Ross

A thesis submitted in partial fulfillment of the
requirements for the degree of

General Engineering

Montana Tech

2016

Abstract

Conductive polymer nanocomposites are a type of particle reinforced plastic composite where the doping material is electrically conductive. The diverse properties of an engineered composite material allow for the material properties to be fine-tuned for the specific application. This research focuses on using carbon allotropes, such as two-dimensional graphene and one-dimensional carbon nanotubes, to achieve direct current electrical conductivity through a polymer fiber. Melt electrospinning is the process used for creating the micrometer scale fibers by melting thermoplastic materials. High electrostatic fields apply a force to the polymer melt and a single fiber is drawn out. The resistivity of the bulk composite and composite fibers were characterized by four-point probe and van der Pauw resistivity measurements. Other material characterization methods such as X-ray diffraction and scanning electron microscopy were used to determine particle size and distribution in the polymer matrix. Several different polymers were used as the matrix material. Originally, the majority of the research focused on relatively low molecular weight varieties of polypropylene. Later, additional polymer samples of recycled polypropylene, polystyrene, and polyethylene terephthalate were supplied in collaboration with the Army Research Laboratory. Premade polypropylene and carbon nanotube composite material were supplied by Sandia National Laboratories and Virginia Tech. The graphene composites utilized polypropylene and polystyrene as the matrix material, and were made at Montana Tech. Recycled polyethylene terephthalate was used to create filament for rapid prototype machines.

Keywords: Melt Electrospinning, Graphene, Carbon Nanotubes, Conductive Fibers

Dedication

I wish to thank my family for all their support and for providing me with the opportunities that began my interest in science.

Acknowledgements

I would like to thank my advisor Jack Skinner for all of his help and direction during both my undergraduate and graduate years at Montana Tech. His knowledge and passion for research has inspired me. I am very grateful for all of the help from Professor Katie Hailer and Professor Brahma Pramanik on my thesis committee and from my friends in the MTNL lab. Lastly, I would also like to thank Sandia National Laboratory and the Army Research Laboratory for funding my research.

Table of Contents

List of Tables

List of Figures

List of Equations

1. Background

Electrically conducting polymer composites (CPC) have recently become interesting materials to study with a variety of applications. The combination of material properties of polymers with the advantage of electrical conductivity found in metals creates a composite material with several applications. N. J. Pinto *et al.* described a process for creating an electronic device with field-effect transistor (FET) semiconducting properties by depositing an electrospun fiber across two gold patterned electrodes on a silicon substrate [1]. Carbon nanotubes have been used to dope polymer coatings for applications in electrostatic and electromagnetic interference shielding [2], increased mechanical properties [3,4], and biosensors [5]. The advancements in CPC's using a biocompatible polymer has led to applications reviewed in Shruti Nambiar and John T.W. Yeow to create biomedical sensors including electrochemical, tactile, and thermal sensors [6]. Inherently conductive polymers also have applications in advancing lithium sulfide battery technology as shown by Yuan Yang, being used as a matrix to hold polysulfide anodes and aid in electron conduction [7]. Although, intrinsically conductive polymers could have been used to form micro- or nano-scale fibers, the main focus of this project is creating polymer matrix composites by doping the polymer with conductive materials.

1.1. Melt Electrospinning

Melt electrospinning (ES) is a manufacturing process first demonstrated in 1936 by Charles Norton [8] as a method to generate polymer fibers with diameters ranging from 10s to 100s of micrometers [9,10]. Melt ES utilizes the liquid phase of thermoplastic polymers by heating the materials above the glass transition temperature or to the melting point, which is an advantage over using harmful solvents with solution ES [10]. The polymer is then delivered to

the tip of a capillary where a high voltage, on the order of 10 kV, is then applied to the capillary and a collection plate is grounded. A large voltage potential between the two electrodes creates an electrostatic force that draws the polymer melt out of the capillary. When the fiber is transferred to the collection plate the polymer melt fibers solidify, creating fibers with micro-scale diameters. The Montana Tech Nanotechnology Laboratory (MTNL) is working on research to develop polymer electrospinning processes as a method for building micro- and nano-scale devices. Incorporating conductive additives into the fibers could lead to the fabrication of future chemical sensors or act as a method for interfacing electronics with the sensors built by the MTNL.

1.2. Polymer Nanocomposites

1.2.1. Polymer Structure

Polymers are one of the three major material categories, the other categories being metals and ceramics [11]. Polymers have a repeating molecular structure, or monomer, that has bonded together multiple times to create a long chained macromolecule. The repetition of the monomer, or the degree of polymerization, can be described by the molecular weight of the macromolecule. Higher molecular weight polymers correspond to longer polymer chains. The structure of the polymer chain is also described by its tacticity which can have an effect on the crystallinity of the overall microstructure with in the material [11].

During this study the majority of the polymers used include Polypropylene (PP), Polystyrene (PS), and Polyethylene terephthalate (PET). Figure 1 below shows the molecular structure of each polymer, PP is on the left, PS is in the center, and PET is on the right.

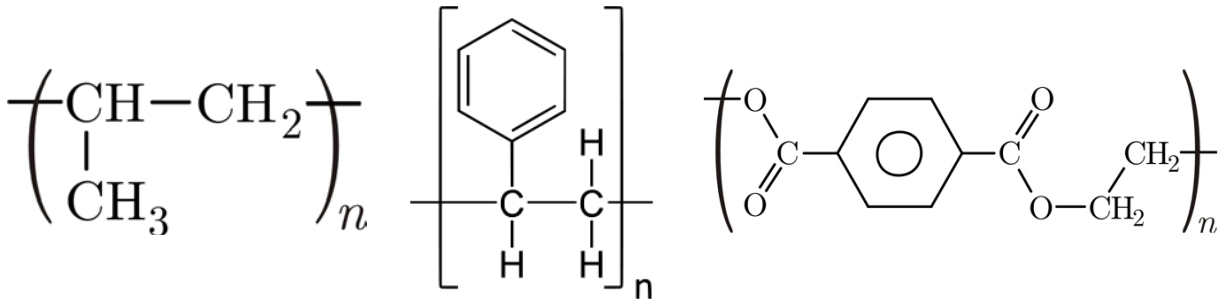

Figure 1: Left, molecular structure of polypropylene (PP). Center, molecular structure of polystyrene (PS). Right, molecular structure of polyethylene terephthalate (PET).

Tacticity is a description of how the pendant group is arranged along the polymer backbone. Polymer chains can be classified as either isotactic, syndiotactic, or atactic [12]. The different tacticity categories are shown for the PS structure in Figure 2.

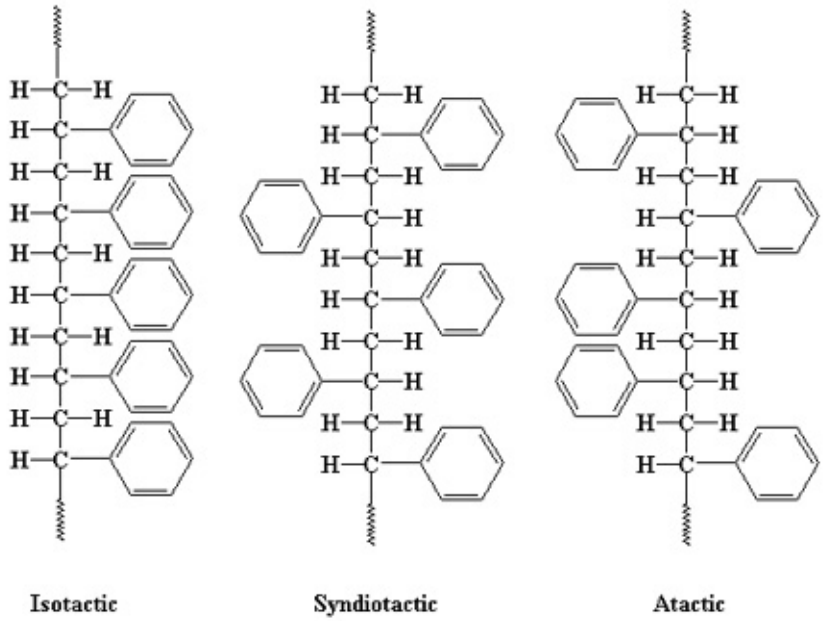

Figure 2: Left, isotactic structure with pendant group on the same side. Center, synidotactic structure with alternating pendant group locations. Right, atactic structure with random pendant group locations.

Isotactic refers to the pendant group being attached to the same side of the polymer chain. A syndiotactic structure has the pendant groups alternating each side of the polymer chain. Atactic structure means that the pendant groups do not have a preferential alignment and are

located randomly on either side of the polymer chain [11,12]. The isotactic structure of PS is only a hypothetical structure to demonstrate the arrangement of pendant groups on the same side of the macromolecule. Isotactic PS is not commercially available and the majority of commercially made PS has an atactic structure.

Tacticity will affect a material's crystallinity. A material's crystallinity is a description of the degree of order found in the material microstructure [11]. When the polymer chains stack in a highly ordered pattern over relatively long distances, as compared to the size of the macromolecules, then the material is described as crystalline and has long range order. Polymer chains that are highly tangled can create a structure that has no order, or long range disorder, and are described as amorphous. Polymers are rarely considered crystalline and usually fall in an intermediate category of semicrystalline structure [13]. Semicrystalline polymers have repeating regions of short range order surrounded by amorphous polymer chains. Figure 3 shows a schematic of a semicrystalline polymer chain structure where crystalline regions are surrounded by amorphous regions.

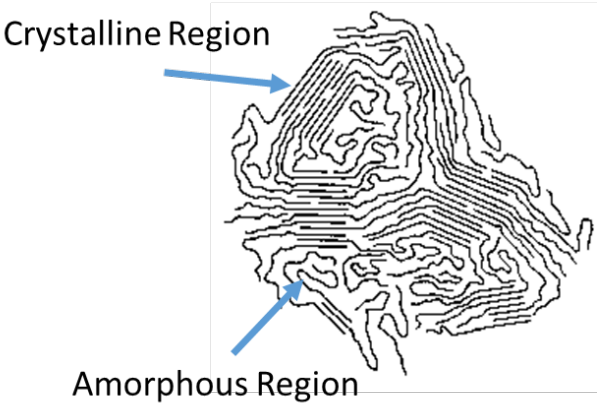

Figure 3: Schematic showing the microstructure of a semicrystalline solid polymer. In a semicrystalline structure there are repeating regions of highly order crystalline material surrounded by amorphous polymer.

The tacticity and crystral structure of the polymer chains has an effect on the material properties. For example, isotactic PP forms a strong and hard semicrystalline solid that has a glass transition temperature of approximately 0 ^{o}C, atactic PP forms a soft and rubbery amorphous solid where the glass transition temperature drops to approximately -15 ^{o}C [14].

1.2.2. Carbon Dopants: CNT, Graphene, Graphite

Although there are a few polymers that are intrinsically conductive, many benefits exist to design a composite to meet the requirements of a particular application. Typically, CPC's are created from a non-conducting polymer and then doped with conducting particles. This was first discovered in 1977 by C. K. Chiang *et al.* when they added p-type dopants to crystalline polyacetylene films [15]. With the addition of more doping material, the space between the conducting particles decreases until there is a continuous path for the current to flow through the material. This is often called the percolation threshold. There have been many studies to determine the percolation threshold for different CPC materials [16-18]. With the recent discovery of carbon allotropes, such as carbon nanotubes (CNT) and graphene, these studies have researched the conducting properties of these new doping materials as well as methods for improving dispersion within the polymer. Graphene is a two dimensional allotrope of carbon with a honeycomb like structure that is one atom thick [19-21]. Graphene can be processed through thermal and chemical graphite exfoliation methods [22]. Previous studies of graphene have shown that it has unique mechanical, thermal, and electrical properties [16-18,23]. A composite material consisting of a polymer matrix and graphene particle filler could be used to increase the DC electrical conductivity of a polymer.

Jing-Wei Shen *et al.* developed a process for improved dispersion of expanded graphite within polypropylene by using solution intercalation [24]. The solution intercalation showed improved conductivity and a lower percolation threshold for the solution (0.67 vol% or ~0.40 wt%) than previous melt mixing (2.96 vol% or ~1.8 wt%) methods. In the solution intercalated study, the polypropylene was dissolved into solution with xylene, and then the suspended expanded graphite solution was added drop by drop. Acetone was then added to force the polypropylene to precipitate. The solution was then heated to drive off the remaining solvent.

Several studies have created conductive micro and nano scale fibers via a solution electrospinning process. Previously several studies demonstrated that carbon nanotubes aligned with the fiber to create conductivity along the fiber length [25]. Qiaoliang Bao *et al.* showed that solution electrospun fibers could be created with polyvinyl acetate and a graphene concentration as low as 0.07 wt% [26]. These fibers exhibited improved mechanical properties as well as a novel process for creating fast photonic devices. As Huan Pang *et al.* achieved a percolation threshold of 0.07wt% of graphene in polyethylene [27], it is possible that the electrospun fibers that Qiaoliang Bao created could be conductive as well. The conductivity measured by Huan Pang *et al.* was on the order of 10^{-4} S/m (resistivity of 1000 Ω-m). To improve the conductivity the CPC's concentration of graphene should be higher. These processes have required that the polymer is dissolved in a solution that often results in strong solvents being released during ES. Solution ES fibers have a large volume loss because of the evaporating solvent resulting in fibers on the order of 10 to 100 nm. Melt ES method used in this study is beneficial because there is no volume loss in the fiber, resulting in fiber diameters larger than solution ES methods. The larger fiber diameters on the order of 10 μm allows for the conductive particles to be contained within the ES fiber.

1.3. Measuring Dopants

1.3.1. X-Ray Diffraction

X-ray diffraction (XRD) is a common method for determining the crystal structure of a material and can be used to characterize unknown materials. Theory of X-ray diffraction is based on wave interference where the two waves with a phase difference can cause constructive or destructive interference. When two coherent X-ray beams are directed at the surface of a material, the diffracted waves will only be inphase when the X-rays interact with the crystal lattice with repeating structure. Bragg's law is the relationship that defines when the diffracted waves will be inphase, shown in equation (1) [28].

$$n\lambda = 2d\ sin\ \theta \quad (1)$$

where λ is the wavelength, n is an integer multiple, d is the lattice spacing, and θ is the angle of incidence

X-ray diffractometers are used to detect the diffracted X-rays. The detector sweeps over a range of angles and gathers intensity data of the diffracted X-rays. Detector position is recorded as an angular position, 2θ, where theta is the angle between the incident beam and the crystallographic plane that causes diffraction.

X-rays are generated by high energy electrons colliding with a positively charged metal anode. When the high energy electrons interact with the atom, an inner shell electron can be ejected. The vacancy created in the inner shell is then filled by an electron from a higher shell and extra energy is released in the form of a photon with characteristic wavelengths in the X-ray range of the electromagnetic spectrum [28]. The X-rays that are generated have a characteristic wavelength depending on the type of target and which electron energy level is filling the inner shell vacancy. Typically, the metal target used for XRD is copper and the electrons interact with the K-shell (or the 1*s* orbital). When electrons from the L-shell (or the 2*p* orbital) fill the vacancy

in the K-shell then Kα X-rays are generated with a wavelength of 1.5406 angstroms. Electrons from the M-shell (or 3*p* orbital) can also fill the K-shell vacancy and generate Kβ X-rays with a characteristic wavelength of 1.3922 angstroms [28].

Most XRD measurements are based on powdered samples so that the examined material consists of a large number of tiny crystals with a random orientation. XRD can also be used to examine how nanoscale materials interact with a bulk material to form a composite. The intensity peak position of the diffracted X-rays will vary depending on the type of micro- or nanocomposite [29]. When the nano-material agglomerates within the matrix material, the XRD spectra will show two distinct phases, which is referred to as a phase separated microcomposite. An intercalated nanocomposite has improved dispersion of the nano-material within the matrix material. For intercalated mixtures the XRD spectra will show a shift in the characteristic peaks to smaller 2θ values because of the increased d spacing between the crystallographic planes. Exfoliated nanocomposites have the highest dispersion and the XRD spectra will show broad peaks, resulting in short range order in the crystallographic planes.

1.4. Electrical Property Measurements

1.4.1. Four-Point Probe Resistivity

Resistivity is an intrinsic material property and is an important value for material and device characterization. Semiconductor resistivity can be measured by either two- or four-probe methods. Typically, the probes are collinear and have equal spacing, where current can be injected and then removed in a straight line along the material. The collinear orientation allows for simplification in calculating the resistivity because of the known geometry. Other probe orientations can be used, but interpreting data becomes more complex. Data from two-probe measurements is also difficult to interpret because the two contacts have multiple functions,

where the current and voltage are measured on the same node, shown in Figure 4 (left) below. For both the two- and four-probe methods the total resistance measured is a function of three resistances: wire resistance, contact resistance, and material resistance. With the two-point probe configuration, it is impossible to determine just the material resistance because the wire and contact resistances are also unknowns [30].

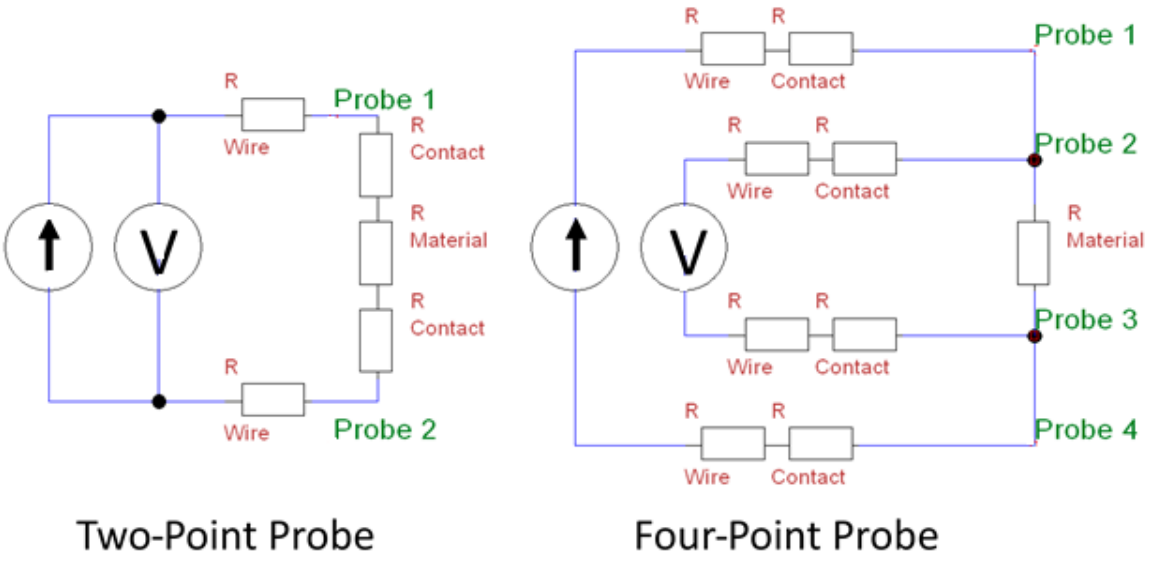

Figure 4: Left, circuit diagram for two-point probe method showing the associated resistances measured as a total resistance. Right, circuit diagram for the four-point probe method showing the voltmeter measuring only the material resistance.

The four-point probe configuration is shown in Figure 4 (right). By adding two probes to measure the voltage, independent from the probes that supply current, material resistance can be determined. Voltmeters are designed to have a high impedance so that a negligible current flows through the meter. Because of this high impedance and small current on the inside loop, there is a negligible voltage drop across the resistances associated with the wire and contacts. The negligible voltage drop means that the wire and contact resistance can be neglected and results in the resistance measured being associated with the material resistance.

To calculate the material resistivity, the general equation is shown below.

$$\rho_o = 2\pi sF\left(\frac{V}{I}\right) \tag{2}$$

where ρ_o is electrical resistivity, *s* is the probe spacing, *F* is a geometry correction factor, *V* is the voltage differential, and *I* is the current injected into the sample

The derivation of the general equation used to calculate the resistivity assumes:

1. Probe tips are infinitesimal;
2. Samples are semi-infinite in the lateral dimensions and probes are placed away from the edges; and
3. For thick samples, thickness is much greater than probe spacing, the current propagates spherically from the outside probe tips.

When the sample thickness is no longer significantly greater than the probe spacing dimension then additional geometry correction factors have to be included in the equation. The type of substrate also becomes important because of the current interaction with the sample and substrate boundary. If the substrate is conductive, current can propagate through the thin sample and leak into the conductive substrate, resulting in a lower resistivity than expected. Equation (3) below shows the geometry correction equation adjusted for a conductive substrate.

$$F_1 = \frac{t/s}{2\,ln\left\{\frac{sinh(t/s)}{sinh(t/2s)}\right\}} \tag{3}$$

where F_1 is the correction factor for a conductive substrate, *t* is the sample thickness, and *s* is the probe spacing

If the substrate is insulating, more current will be contained within the sample film and will prevent the current for completely propagating throughout the sample. Equation (4) shows the geometry correction for an insulating substrate.

$$F_2 = \frac{t/s}{2\,ln\left\{\frac{cosh(t/s)}{cosh(t/2s)}\right\}} \tag{4}$$

where F_2 is the correction factor for an insulating substrate, t is the sample thickness, and s is the probe spacing

When the sample thickness is approximately half the probe spacing, ($t \leq s/2$) the correction factor can be simplified to Equation (5), which shows the general resistivity equation adjusted for an insulating substrate.

$$\rho = \frac{\pi}{ln(2)} t \left(\frac{V}{I}\right) \tag{5}$$

where ρ is electrical resistivity, t is the sample thickness

Additional geometry correction factors can also be applied to correct current and voltage measurements when the other assumptions are not fully satisfied. For example, there are similar correction values used for the lateral dimensions when the sample is no longer considered to be semi-infinite.

For thin films ($t << s$) the material is often characterized by the sheet resistance. Sheet resistance can also be calculated from the current and voltage data generated in a four-point probe measurement.

$$R_{sh} = \frac{\rho}{t} = \frac{\pi}{ln(2)} \frac{V}{I} \tag{6}$$

where R_{sh} is the sheet resistance

Equation (6) shows the sheet resistance calculation and is relation to resistivity. Sheet resistance is dependent of thickness and has units of ohms per square (Ω/□)

1.4.2. Van der Pauw Resistivity

Semiconductor resistivity of an arbitrary shape can also be determined by using the van der Pauw method typically used for conformal mapping and utilizes the Hall Effect theory [31]. The Hall Effect is a phenomenon where a voltage potential is generated perpendicular to the current flow. Common van der Pauw structures used to characterize a bulk material resistivity or a thin film sheet resistance include the Greek cross structure. Symmetry of the cross allows for the current to flow along the vertical component while the hall voltage is measured across the perpendicular component.

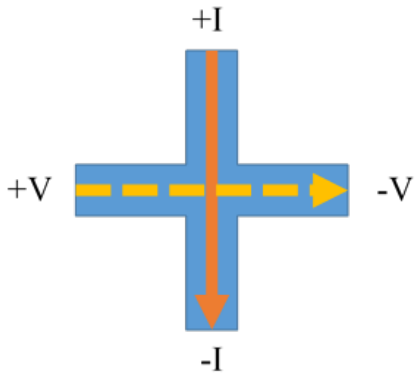

Figure 5: Van der Pauw Greek cross structure diagram showing the injected current flowing through the vertical component and the corresponding Hall voltage being measured in the horizontal component.

The van der Pauw method can be used to calculate an average material resistivity by changing the orientation of the current and voltage probes. Average resistivity values are helpful in characterizing materials with heterogeneous loading of conductive particles.

The van der Pauw method is valid for the conditions where:

1. The contacts are at the circumference of the sample;
2. The contacts are sufficiently small;
3. The sample is homogenous in thickness; and
4. The surface of the sample is singly connected, i.e. does not have isolated holes.

When the conditions stated above are met, the relation shown in Equation (7) can be used to find a material resistivity [30].

$$e^{-\left(\pi\frac{d+R_{AB,CD}}{\rho}\right)} + e^{-\left(\frac{d+R_{CD,AB}}{\rho}\right)} = 1 \tag{7}$$

where d is the structure thickness, R is the resistance measured, and ρ is the resistivity

The relation shown in Equation (7) can be rearranged, simplified, and solved for resistivity as shown in Equation (8) below.

$$\rho = \frac{\pi}{\ln(2)} d \frac{R_{AB,CD} + R_{CD,AB}}{2} \tag{8}$$

where ρ is the electrical resistivity for the Greek cross van der Pauw structure

2. Methods

2.1. Material Processing

To create the conductive electrospun fiber composite, the materials that were used included: 14,000 molecular weight atactic polypropylene and graphene nanoplatelets from ACS Materials. Atactic polypropylene was chosen because of its ability to be completely dissolved into solution with toluene [32]. An 18 wt% solution of PP and toluene was created by placing the polymer beads into a flask and stirred while being heated at 80 ^{o}C. Once the polymer was completely in solution it was added to a specific weight of graphene nanoplatelets to create a 6 wt% mixture. Then an ultrasonic probe was used to mix the solution of graphene and PP in toluene. Sonication also helped to break up the agglomerations of graphene to increase dispersion. The ultrasonic probe was set to a power of 450 watts (75% of the maximum power) and applied at one minute intervals. A sample of the graphene and PP solution was removed between each interval and then prepared for melt electrospinning. Samples were then drop cast in to a thin film in a glass petri dish so that the remaining solvent could be removed by evaporation.

2.2. Melt Electrospinning

Electrospinning conductive polymers introduced the challenge of the fiber creating a short between the two electrodes and resulting in damaged fibers. A structure was created to support substrates and keep them a safe distance away from the electrodes to prevent electrical breakdown. The key requirement for the design of the support structure was to use materials with a low electrical resistivity so that the structure has a minimal impact on the electric field. The fibers were then collected on to a glass microscope slides on the mid-plane collection device.

2.3. Bulk Electrical Properties

2.3.1. Four Point Probe Resistivity

To test the electrical conductivity of graphene and PP mixture, thin film samples were created for measuring resistivity with the four-point probe method. Four-point probe electrical measurements are common material characterizing technique to extract a materials electrical resistivity. Four-point probes are typically set in a collinear orientation with equal spacing between each probe. The outer most probes are used to inject a current, while the inside probes are used to measure a differential voltage, as shown in Figure 6 below. Current will propagate spherically away from the tip of probe one and spread through the material film until it reaches probe four. Because of the thin sample thickness that confines the current as it travels through the material there is a need for correction factors to account for the geometry of the sample. Equation (9) blow is valid for geometries where the sample is semi-infinite in the lateral directions away from the probes, and that the sample thickness is greater than twice the probe spacing.

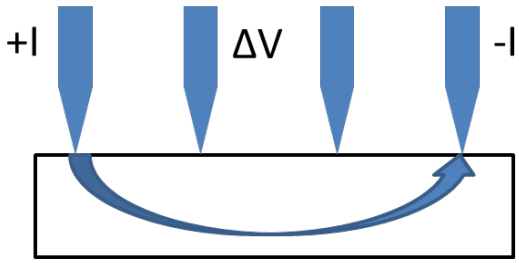

Figure 6: Four-point probe schematic showing the configuration of the electrical probes and the current spreading through the material sample.

$$\rho_o = 2\pi s\left(\frac{V}{I}\right) \tag{9}$$

where ρ_o is electrical resistivity, s is the probe spacing, V is the voltage differential, and I is the current injected into the sample

To adjust the resistivity measurements for a thin film, a correction factor term needs to be added to the original equation. The corrected equation is shown below and is now applicable for thin samples of semi-infinite lateral dimensions on a non-conductive substrate.

$$\rho = \frac{\pi t}{\ln(2)}\left(\frac{V}{I}\right) \tag{10}$$

where ρ is the corrected electrical resistivity for the sample thickness t

The current and voltage data was logged using a Keithley 2450 source-measure unit. Multiple data sets were then imported into a MATLAB script that averaged the data and then calculated resistivity.

2.3.2. Van der Pauw Resistivtiy

Van der Pauw structures are another common method in the semiconductor industry for measuring a materials resistivity. The van der Pauw technique utilizes the Hall effect to determine the resistivity and can be used with arbitrary sample geometries. Greek cross structures were used to simplify the geometry. An electrical current was injected through the one component of the Greek cross and the Hall voltage was measured in the perpendicular component. Symmetry of the Greek cross van der Pauw structure allows for multiple contact configurations, and by averaging the values from multiple configurations, a more consistent value for resistivity can be achieved. Below in Figure 7 are examples for two of the possible eight contact configurations used with the Greek cross structure.

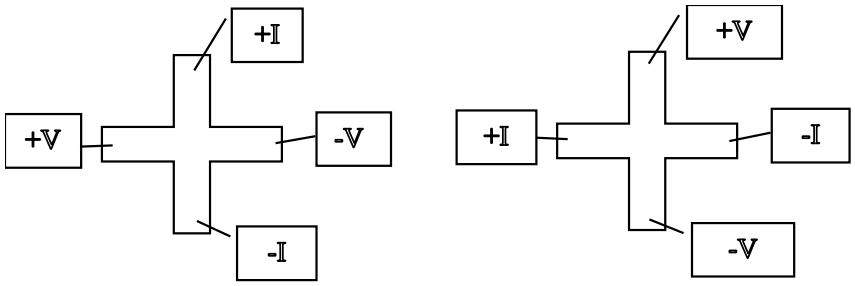

Figure 7: Van der Pauw Greek cross structure diagram representing the multiple electrode configurations used to find an average material resistivity. By changing the direction of the current flow through the Greek cross structure multiple values can be averaged together and provide a more accurate resistivity value for non-homogenous materials.

Material resistivity could be calculated by using the relation described earlier with the simplified equation shown below. The subscript notation used with the resistance measurement means that current is flowing from points A to B and the voltage is measured from points C to D.

$$e^{-\left(\pi\frac{d+R_{AB,CD}}{\rho}\right)} + e^{-\left(\frac{d+R_{CD,AB}}{\rho}\right)} = 1 \tag{11}$$

where d is the structure thickness, R is the resistance measured, and ρ is the resistivity

$$\rho = \frac{\pi}{\ln(2)} d \frac{R_{AB,CD} + R_{CD,AB}}{2} \tag{12}$$

where ρ is the electrical resistivity for the Greek cross van der Pauw structure

A study to determine the accuracy of the four-point probe and van der Pauw resistivity values was completed by comparing the percent difference between the resistivity values obtained by each method. Samples of CNT doped PP were prepared by Virginia Tech as a collaboration with Sandia National Laboratories (SNL). A small sample of PP/CNT composite was melted to form into both bulk films and Greek cross van der Pauw structures and then were tested.

2.4. Fiber Electrical Properties

The material was electrospun into fibers, and the resistivity was measured along the length of the fiber. To measure the fibers resistivity, a Signatone micromanipulator probe station was used to land four tungsten probes along the length of the fiber at uniform distances. Then using the same principle of the four-point probe method, the current and voltage data could be measured. By assuming all of the current is contained within the fiber, a resistivity could be calculated. Data generated from these measurements included voltage and current which allowed for resistivity to be calculated. Equation (13) was rearranged to solve for resistivity.

$$R = \rho \frac{L}{A} \rightarrow \rho = \frac{RA}{L} \tag{13}$$

where R is the resistance of the fiber, ρ is the resistivity of the material, A is the cross sectional area, and L is the distance along the length of the fiber between the two voltage probes

3. Results

3.1. Melt Electrospinning Tool Modifications

Further modifications have been made to the melt electrospinning tool since the senior design project was completed. Much of the functionality remained the same, but small modification were done to have improved control. These modifications include: ceramic insulated spinneret, finely honed melt chamber wall, and manual air pressure adjustment.

3.1.1. Spinneret Ceramic Insulator

Pottery clay was used to create an insulator and was fired in the muffle furnace at 950 ^{o}C for 60 minutes. The program for the muffle furnace is shown in Table I below.

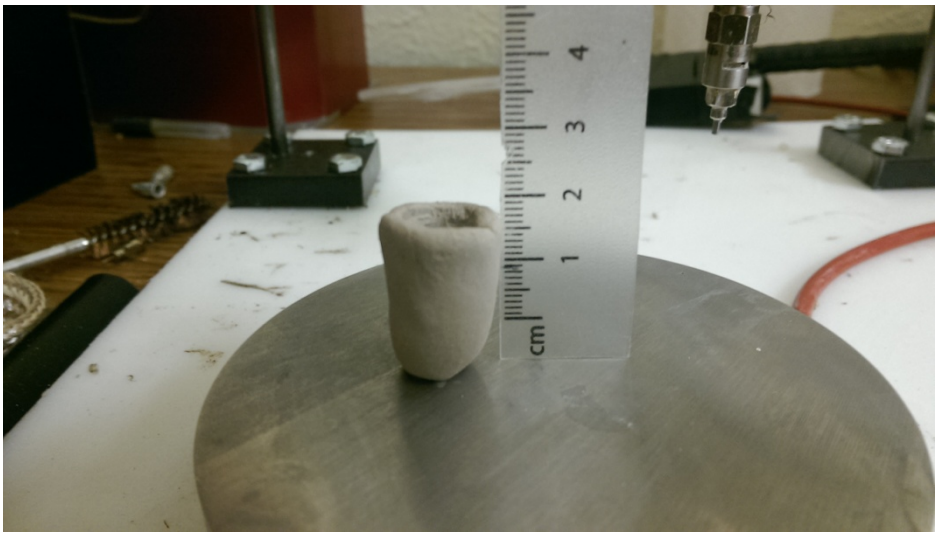

Figure 8: Ceramic insulator for melt spinneret. The insulator was made to retain heat in the exposed electrospinning needle.

The insulator was designed using a rough estimation for shrinkage, approximately 1/8 inch per inch of material, and was fired at 950 degrees C. Most pottery clay sintering occurs at

900 ºC, and 950 ºC is a commonly used temperature. The program for the muffle furnace was adjusted to allow for the 10ºC/min and is shown in the table below.

Table I: Muffle furnace program values, 950 ºC for 60 min.

C01	0
T01	95
C02	950
T02	60
C03	950
T03	-121 (end program)

The ceramic insulator appeared to completely sinter and formed a tough ceramic that fit well on the spinneret of the melt electrospinning tool. Testing of the insulator demonstrated that the spinneret was able to maintain a higher steady state temperature than the previous configuration with an exposed metal surface.

3.1.2. Melt Chamber Hone

Machined surfaces of the melt chamber wall were originally rough because of the work hardening properties of stainless steel. The chamber was polished with both a coarse and fine grit ball hone made for brake cylinders, the coarse hone was 120 grit and the fine hone 320 grit. After honing, the surface roughness was significantly decreased and had smooth actuation of the piston in the melt chamber. Once any melted polymer was added the chamber, the friction increased significantly and caused problems for the closed loop feedback air pressure system.

3.1.3. Manual Air Pressure Adjustment

A closed loop feedback pressure controller used a PID controller to regulate the pressure that was applied to the pneumatic piston. Initially, the reaction time of the PID controller was too slow and did not have the fine adjustments required for suppling a controlled feed rate of polymer to the spinneret. The main obstacles that prevent the PID controller from operating

correctly is the alignment of the melt chamber with the piston and the high friction between the melted polymer and the cylinder wall. To overcome the high friction, the piston needs to have a sharp impulse of force to overcome the static friction and then quickly reduce the pressure to prevent all of melted polymer from being forced out the spinneret. A complex control system could be designed to supply the impulse required to get the piston moving but a simple manual control was implemented.

The manual air pressure control consist of a blow off ball valve located on the compressor exit before the four-way position valve. By closing the ball valve, the flow rate of air is adjusted and the pressure spikes enough to get the piston moving. Opening the ball valve allows for the air pressure to be released and reduces the feed rate of the polymer at the spinneret tip. This simple manual control presents the disadvantage of inconstant feed rates that changes the quality of the electrospun fibers. The effect of feed rate on the fiber quality is most noticeable with low viscosity polymers because of the low shear stress required for the polymer melt to flow. High viscosity polymers require a higher shear stress for the polymer melt to start flowing and naturally dampens the inconstancies with the manual air pressure control.

3.1.4. Mid-plane Collector

For electrospinning conductive polymers, a mid-plane collector was made to support glass slides off of the charged electrode. Without the mid-plane collector, the electrospun fibers would cause electrical breakdown between the fiber and the charged electrode. Once current began to flow through the fiber, Joule heating would destroy the fiber.

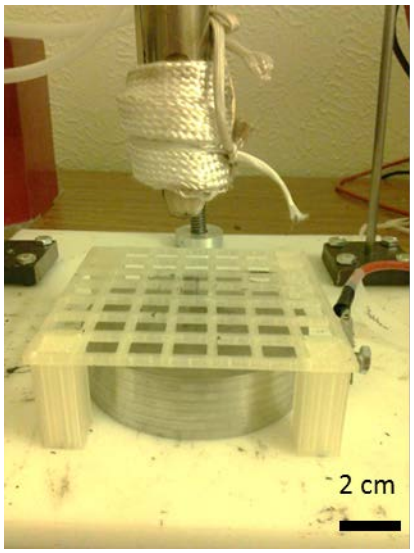

Figure 9: Mid-plane collector for electrospinning conductive materials onto glass microscope slides to prevent electrical breakdown and current flow through the fiber.

Figure 9 shows the rapid manufactured part used to support glass microscope slides way from the charged electrode. The grid of the mid-plane collector was designed with the intent of having minimal impact on the electric field.

3.2. Characterizing Temperature Control

To characterize the temperature gradient across the melt chamber, temperatures were recorded for a given set point on the temperature control system and then compared to a model. Temperature measurements were taken with a K-type thermocouple on a digital multi-meter at locations along the length of the melt chamber. The temperature control system was set to a set point of 75 ^{o}C and allowed to reach a steady state condition. Then, the temperature was recorded for several locations along the length of the melt chamber. Location 1, was at the tip of the spinneret. Locations 2-7, corresponded to the exposed metal above the heating element with ½ inch increment spacing moving away from the heating element. Location 8, was the maximum temperature recorded on the surface of the heating element and was also used as the error to provide feedback control to the PID controller. Also, the room temperature of the air was

measured to provide a value for the convective heat transfer model. Table II shows the recorded temperatures along the length of the melt chamber when heated to the proper temperature to melt ES low molecular weight PP.

Table II: Measured melt chamber temperatures with a set point of 190 ºC

Location	Temperature(ºC)
1	120
2	148
3	130
4	120
5	110
6	101
7	95
8	191
Air	23

A model for the heat transfer in the melt chamber was created using Creo Parametric (formerly Pro/Engineer). The assumptions for heat transfer coefficients started with close approximations, and small adjustments were made until the model matched closer to the temperatures that were previously measured in Table II above. Once the heat transfer coefficients were determined the prescribed temperature was adjusted to a value used for real melt ES conditions and compared to the results to the other measured temperatures. Figure 10 shows a schematic of the boundary conditions that were applied to the model in order to determine the temperature gradient throughout the melt chamber.

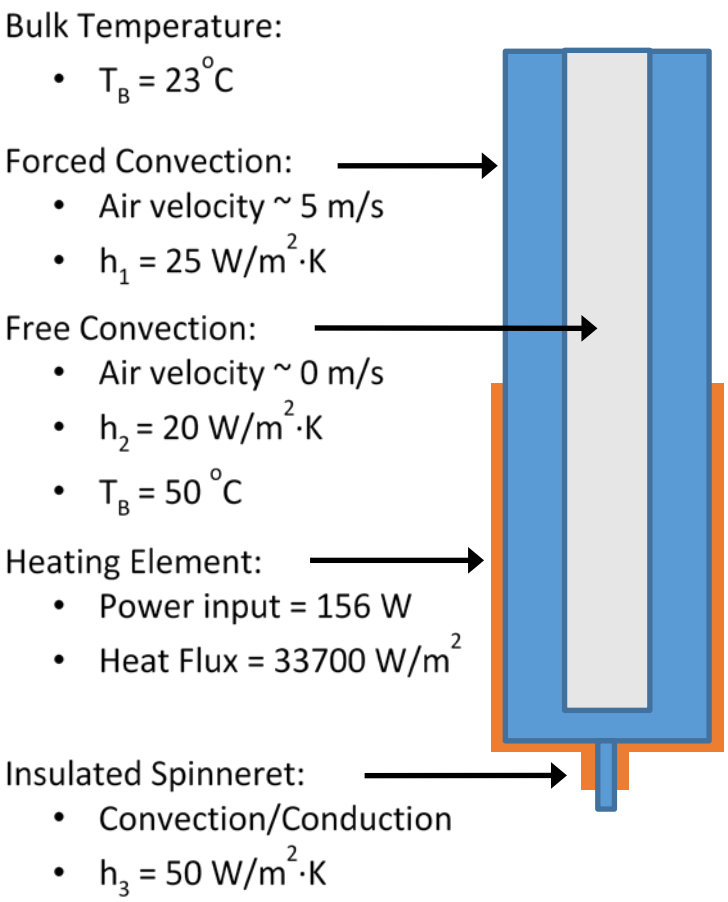

Figure 10: Schematic of the melt chamber heat transfer model with labeled boundary conditions used to predict the temperature gradient.

Model assumptions and boundary conditions:

- The area wrapped with the heating element is set at a prescribed temperature (the control system set point)
- Top half of the melt chamber is forced convection heat transfer:
    - Air velocity ~ 5 m/s
    - Convection heat transfer coefficient, h_1=25 W/m^2 K
    - Bulk Temperature, T_B= 23^{o}C
- Inside of the melt chamber is free convection heat transfer:

- Air flow is negligible
- Convection heat transfer coefficient, h_2=20 W/m^2K
- Bulk Temperature, T_B= 50^{o}C

- Heat transfer at the melt chamber tip is a combination of convection and conduction:
  - Modeled as convection with a greater coefficient than the forced convection condition.
  - Convection heat transfer coefficient, h_2=50 W/m^2K
  - Bulk Temperature, T_B= 23^{o}C
- Heat flux input:
  - Heating element total power=156 W
  - Heat flux=Power/Area =33700 [W/m^2]

The heat transfer model was ran with the boundary conditions listed above and compared with measured values. Table III show the results of the model with a set point value of 150 ^{o}C. In the heat transfer model, the locations could only be approximated so a range was reported only for the easiest to read.

Table III: Heat transfer model results for a set point of 150 C and compared to measured values.

Location	Temperature (°C)	Model Temperature (°C)
1	102	102-107
2	118	120-118
3	101	
4	89	
5	81	
6	74	
7	69	70-64
8/ Set Point	156	
Air	23	

Figure 11 shows a representation of the temperature gradient across the melt chamber and can be used to estimate temperatures.

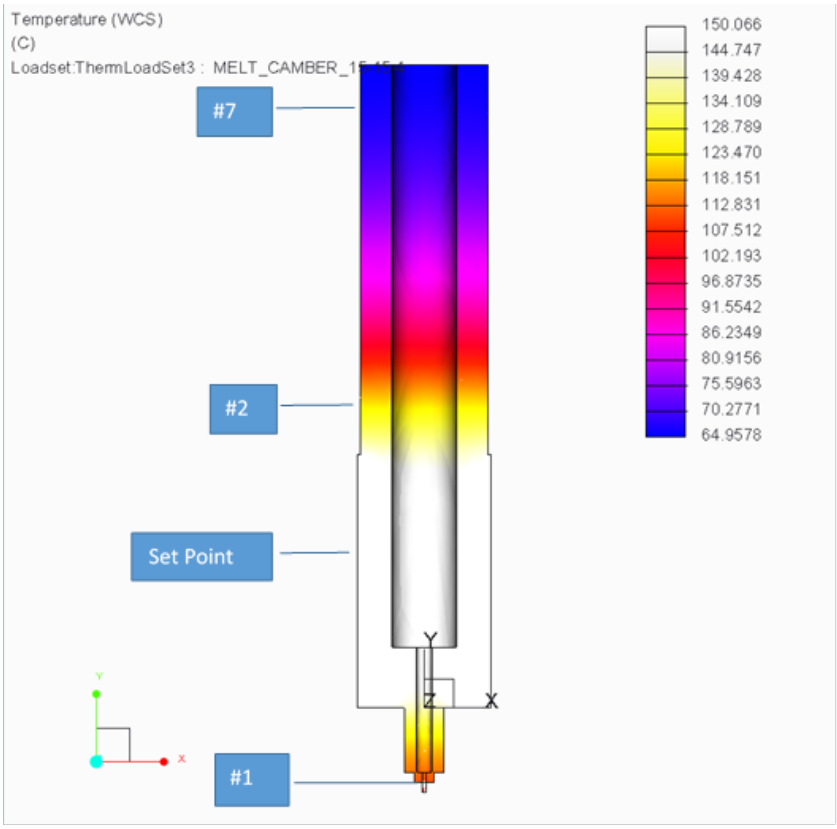

Figure 11: Heat transfer model representation of the temperature gradient with a set point of 150 °C

The model was repeated for a set point of 190 ºC. Results are shown below in Table IV, and the temperature gradient is shown in Figure 12 below.

Table IV: Heat transfer model results for a set point of 190 ºC and compared to measured values.

Location	Temperature (ºC)	Model Temperature (ºC)
1	120	133-126
2	148	154-147
3	130	
4	120	
5	110	
6	101	
7	95	83-76
8/ Set Point	191	
Air	23	

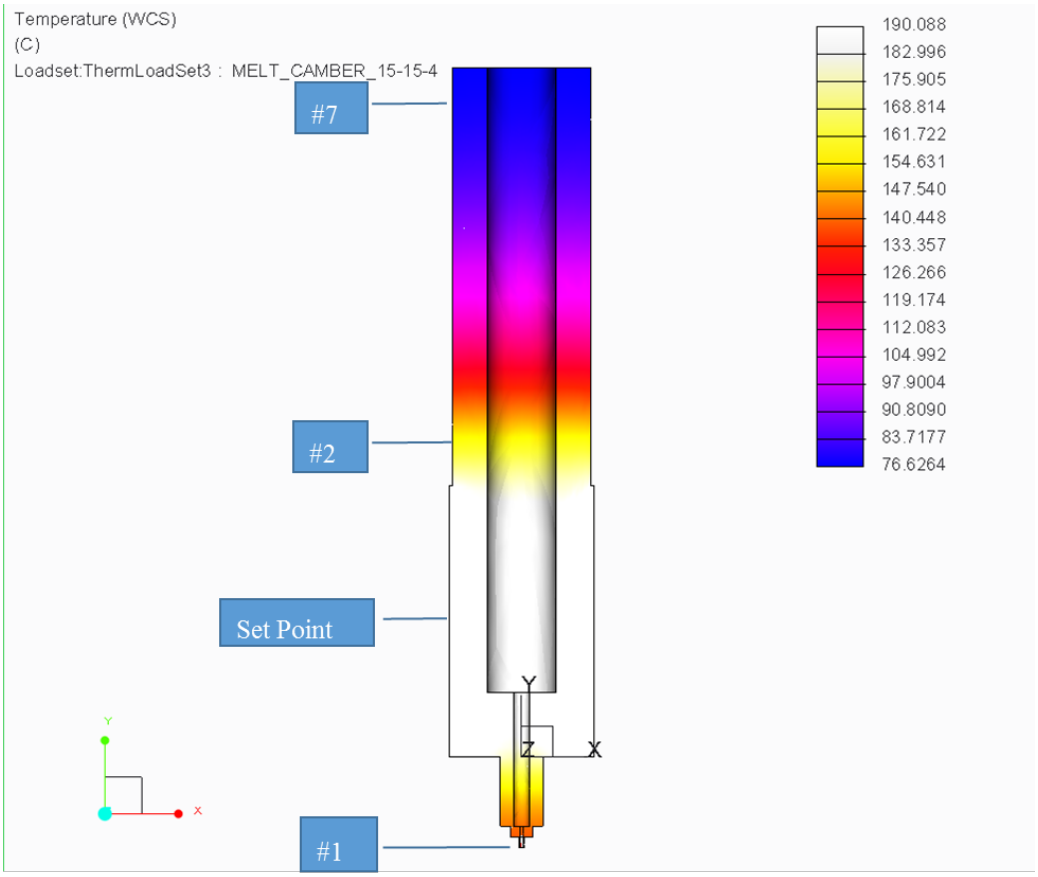

Figure 12: Heat transfer model representation of the temperature gradient with a set point of 190 ºC

The final model run was repeated for a set point of 220 ºC. Results are shown below in Table V, and the temperature gradient is shown in Figure 13 below.

Table V: Heat transfer model results for a set point of 220 ºC and compared to measured values.

Location	Temperature (ºC)	Model Temperature (ºC)
1	150	161-152
2	182	186-178
3	162	
4	143	
5	140	
6	120	
7	115	93-85
8/Set Point	221	
Air	23	

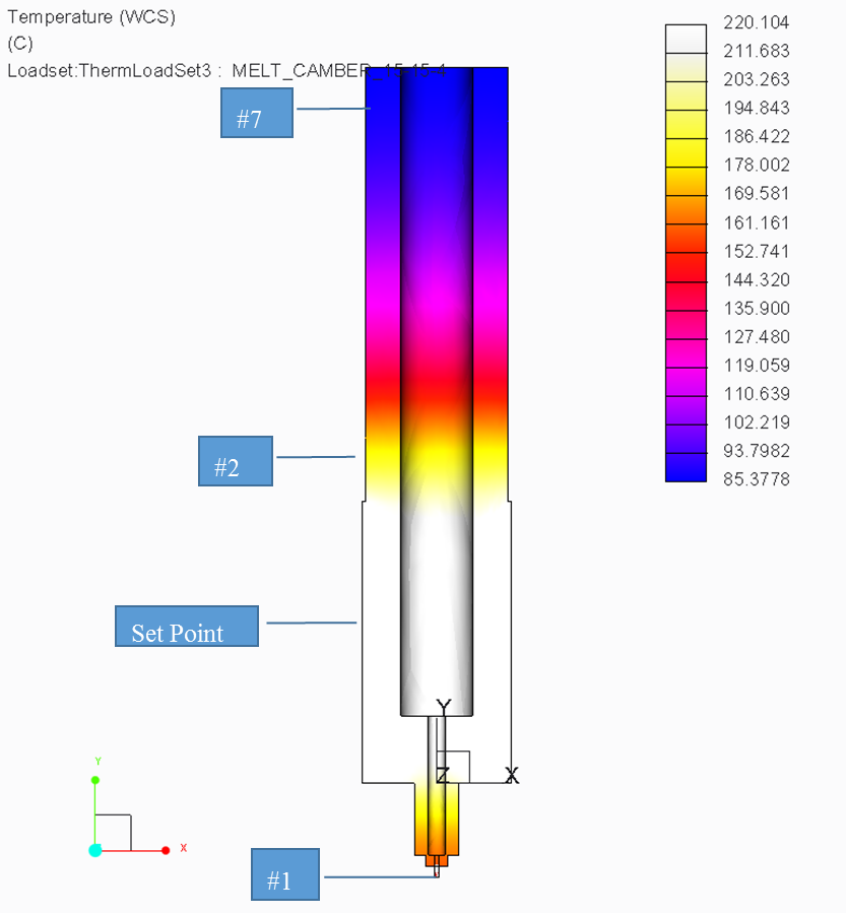

Figure 13: Heat transfer model representation of the temperature gradient with a set point of 220 ºC

Further testing has been conducted with a Resistance Temperature Device (RTD) temperature probe inside the melt chamber. The RTD temperature measurements has shown that the inside of the chamber is approximately 10 ^{o}C higher than the set point at the surface of the heating tape.

3.3. Material Preparation

The melt electrospinning tool has a chamber diameter of ½ inch. This allows for the melt chamber to be filled by either polymer pellets or ½ inch diameter sticks up to 4 inches in length. Previous material was supplied by SNL in the form of ½ inch diameter sticks. Therefore, a mold was created to cast polymer sticks from materials made at Montana Tech. The mold was made on a Haas Computer Numeric Control (CNC) mill and machined from a piece of aluminum with a 2-3/4 inch long slot and the two mold halves bolt together with ¼ inch bolts. The mold is shown in Figure 14.

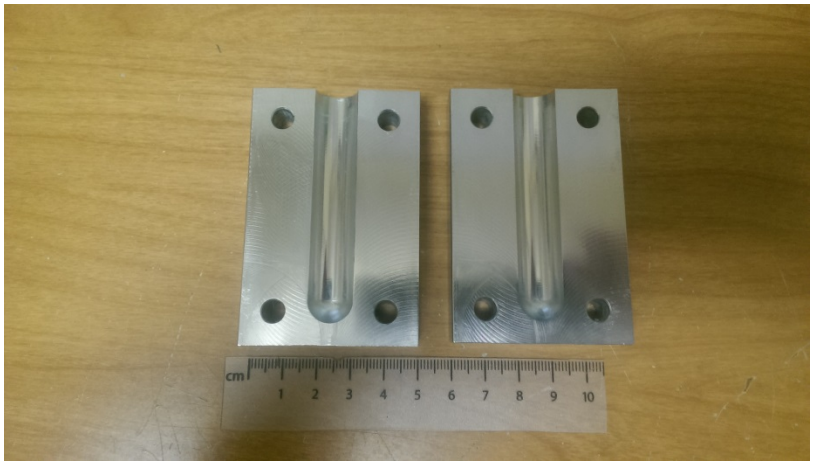

Figure 14: Aluminum mold for ½ inch polymer sticks.

A mold release coating was applied to the mold halves to allow for easy removal of the sticks. Aluminum metal polish was first applied to remove the oxide layer and provide a clean

surface for the mold release. The mold release used was FibRelease and was applied with a paper towel and allow to air dry. The mold release was applied three times to form a thick layer.

Heat was applied to the mold by wrapping it with flexible heating tape and connected to the melt electrospinner temperature control system. The mold and heater element set up is shown in Figure 15 below.

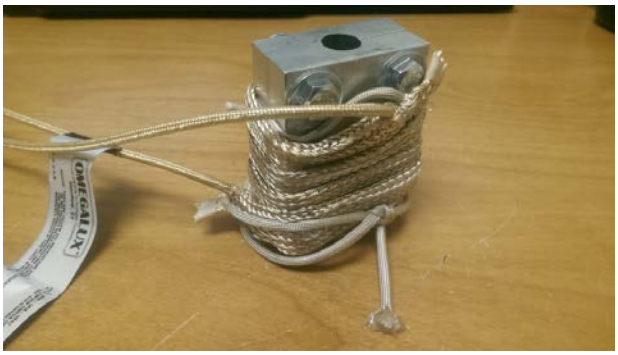

Figure 15: Polymer stick mold and heating element controlled by Melt ES temperature system.

After the mold has reached the proper temperature, the polymer pellets were added. Waiting to add the polymer pellets prevented the material from degrading if the temperature was set too high. In the first trial 14k MW PP pellets were added to the mold and stirred. When completely melted the PP was clear and solidify to an opaque white. The power was then turned off and allow to cool for approximately 20 minutes. The polymer stick is shown in Figure 16 after cooling.

Figure 16: Final polymer stick and mold after cooling.

Figure 17 shows the final polymer stick removed from the mold. The final diameter was 0.490 inch, which provided enough clearance to be feed into the melt chamber while adding minimal amounts of air once the piston sealed behind the stick.

Figure 17: Final product of 14k MW PP stick prepared for feeding into melt chamber.

Polymer sticks were also created for the other materials used with the melt ES tool. Figure 18 shows the process of heating and temperature control to final cast sticks. The image on the right in Figure 18 are polymer sticks made from recycled PP, PS, and PET from left to right. The materials used were supplied in collaboration from the Army Research Laboratory (ARL).

Figure 18: Polymer stick molding process for ARL supplied recycled materials. Left, mold heating and temperature control. Middle, cast polymer stick in mold. Right, recycled PP, PS, and PET from left to right.

3.4. Melt Electrospinning Polymers

The main thermoplastic polymers used with the melt ES tool include PP, PS, and PET. Initial melt ES was performed with low molecular weight PP which included both 12,000 MW atactic and 14,000 MW isotactic verities. Collaboration with ARL added the use of recycled materials, which included extrusion grade, high molecular weight PP, PS, and PET. The PS was measured by ARL to have a molecular weight of 220,000. High molecular weight polymers were able to be electrospun and produced fiber diameters from approximately 20 microns down to 5 microns depending on the polymer type and the process parameters. Melt ES parameters were similar for both the PP and PS whereas the PET had to be electrospun at higher temperatures. The temperature was set to 180-200 ^{o}C, voltage was between 7.0-9.0 kV, and a separation distance of 2.5 cm. Figure 19 shows optical micrograph images of electrospun recycled PP. When electrospinning at higher temperatures and low feed rates the PP began to electrospray.

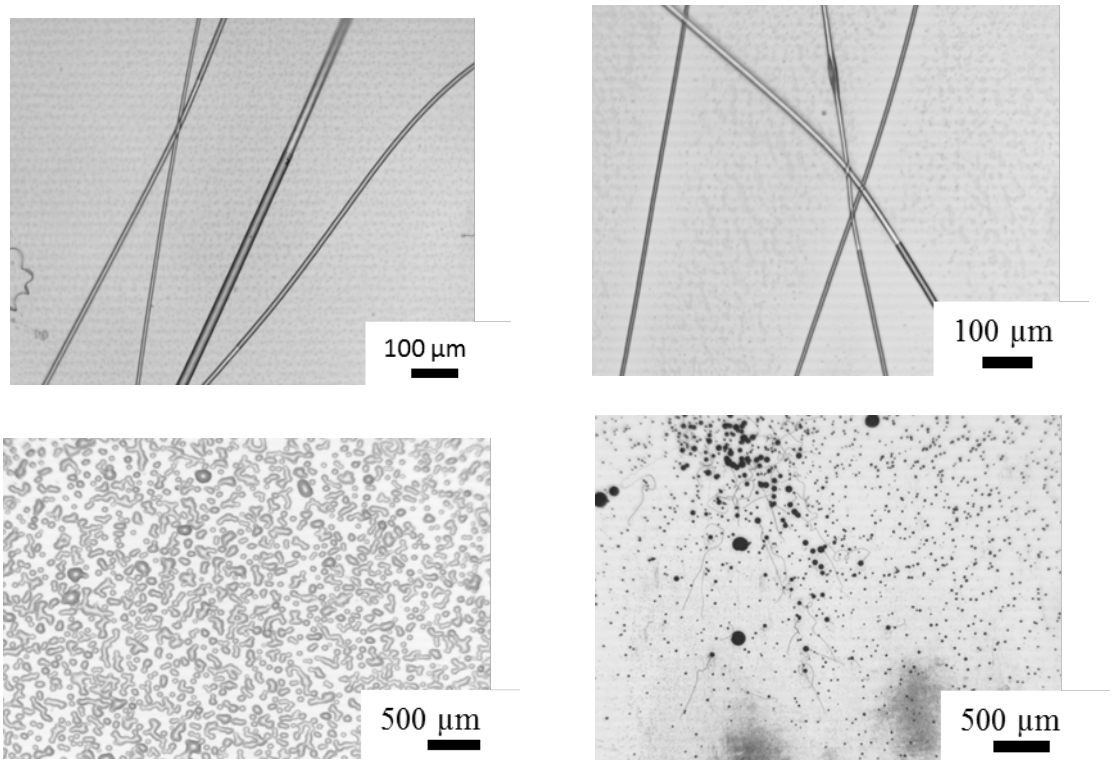

Figure 19: Recycled PP electrospun fibers (top) and electrospray droplets (bottom).

Figure 20 shows optical micrographs of the recycled PS fibers. The majority of the fibers were between 10.0 and 1.0 micron diameters while some of the larger fibers were approximately 88.0 microns. ES fibers made from PS appeared to be nearly transparent and had a smooth morphology.

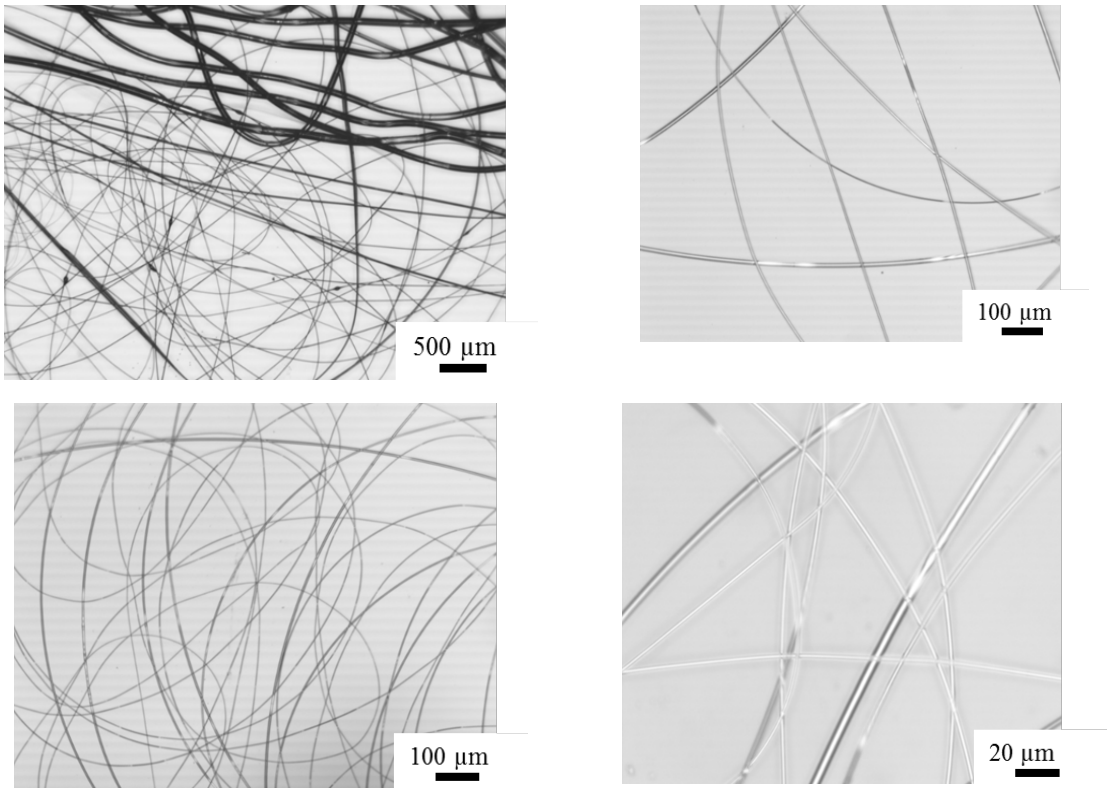

Figure 20: Recycled PS electrospun fibers. Top Left largest fiber diameter approx. 88.0 microns. Other fiber diameters from 1.0 to 10 microns.

Figure 21 shows the electrospun fibers made from recycled PET, which was processed at a higher temperature than the PP and PS, approximately at 250 ^{o}C. The PET fibers had a diameter of approximetly 15.0 microns with occasional fiber diameters of 1.0 to 5.0 microns. PET fibers also appear to have transparent properties associated with an amorphous phase.

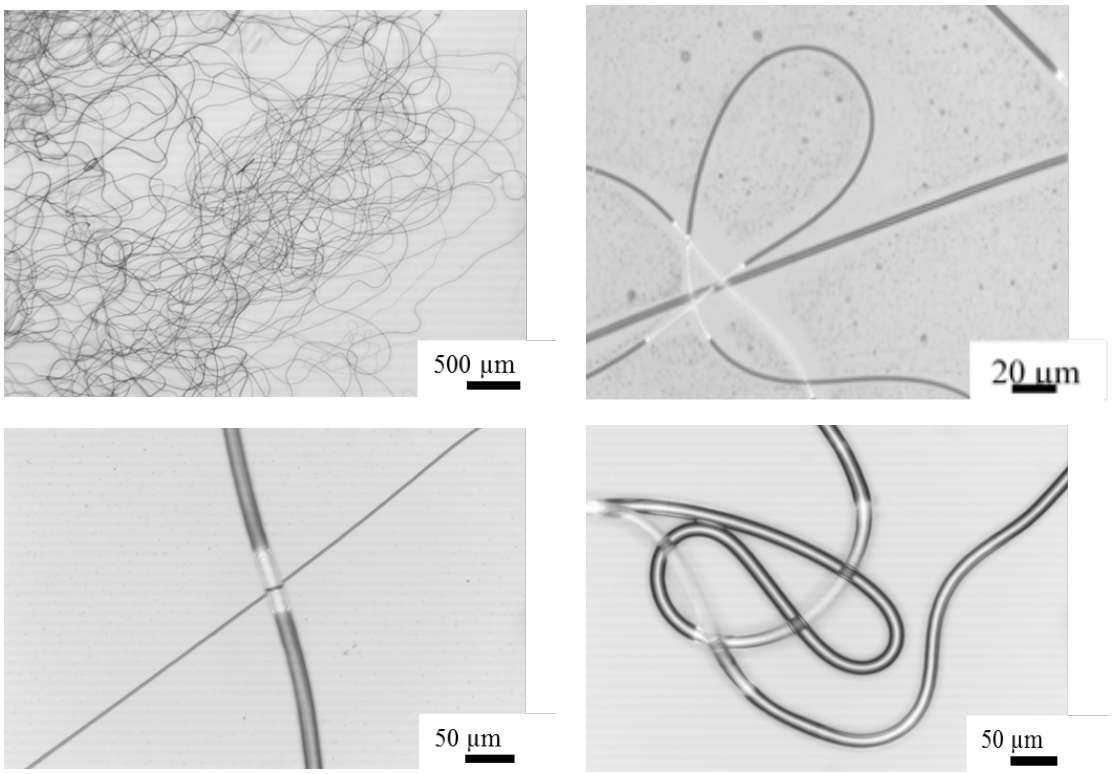

Figure 21: Recycled PET electrospun fibers with diameters of approx. 15.0 microns with the smallest on the order of 1.0 to 5.0 microns.

3.5. Graphene Processing

For this work, two sources of graphene were used as dopants in the polymer matrix. The first source had limited specifications provided but the Petrov Nano Graphene Platelets (NGP) were thermally exfoliated from graphite powder and were not functionalized. The second source of NGPs was from ACS Materials and the provided material properties are shown in Table VI, the electrical conductivity of $8x10^{4}$ S/m is equivalent to an electrical resistivity of $1.25x10^{-5}$ Ω m.

Table VI: Material Properties of ACS Materials supplied NGPs

Diameter	Thickness	Specific Surface Area	Electrical Conductivity
~5 microns	2-10 nanons	20-40 m^2/g	80000 S/m

Both sources of NGPs did not have additional functionalization after they were produced. Without the functionalization the sheets of graphene naturally agglomerate and make weak van der Waals bonds between each sheet, similar to those found in graphite. To prevent agglomeration the NGPs were dispersed in a polar, non-aqueous solvent, and an ultrasonic probe was placed into the solution until most of the agglomeration had been removed. To determine the agglomeration size, a sample was pipetted out, placed on a glass slid, dried, and imaged with an optical microscope. The samples were prepared quickly to limit the agglomerations from reforming.

3.5.1. Graphene Agglomeration Characterization

The ultrasonic probe was set for 150 W, or 25% of the total power, and a timer for 1 minute intervals with a 10 second rest. Samples were taken at each minute of sonication for 5 minutes. The images taken with the optical microscope were then analyzed with ImageJ software to count the number of agglomerations and calculate an area for each agglomeration. Figure 22 shows the optical microscope images of the NGPs agglomerations at 1 minute intervals. The bottom image is a sample of the binary image generated in ImageJ that was then used to count and measure areas of each agglomeration. After 2 minutes the images had minimal visual changes but were still processed in ImageJ.

No sonication

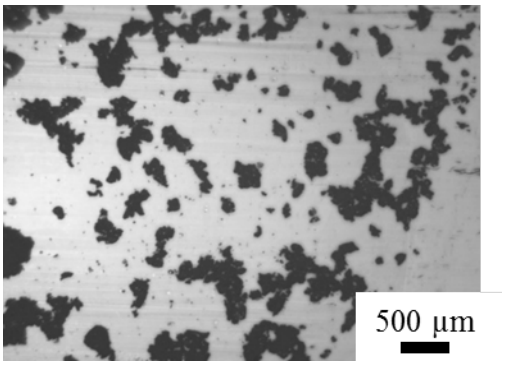

1 min

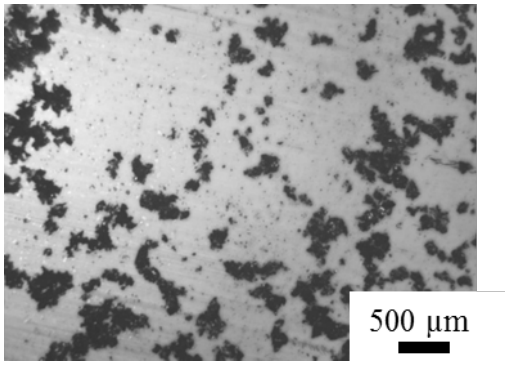

2 min

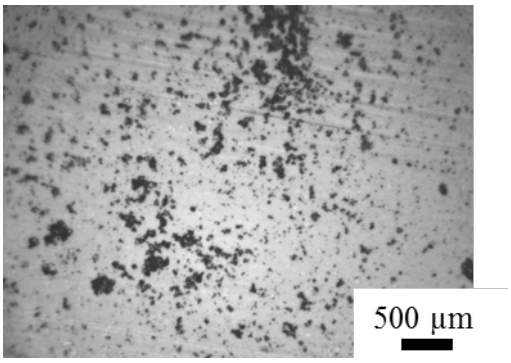

2 min after
ImageJ analysis

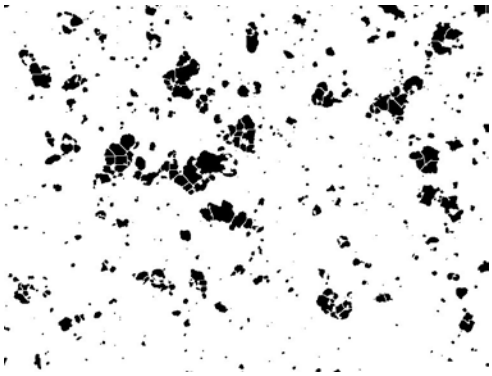

Figure 22: Graphene agglomerations at 1.0 min time intervals after sonication at 150 W. Bottom, binary image processed by ImageJ.

After a binary image (black or white pixels) was created, the Analyze Particles tool in ImageJ was used to automatically identify the particles and determine the area of each particle. Average particle area was then calculated. Table VII below shows the results of the ImageJ analysis.

Table VII: ImageJ particle count results for each minute of sonication.

Time (min)	Count	Total Area (µm^2)	Avg. Area (µm^2)
0	215	4.22E+06	1.96E+04
1	329	1.96E+06	5.97E+03
2	970	1.75E+06	1.80E+03
3	550	9.05E+05	1.65E+03
4	476	8.02E+05	1.68E+03
5	324	7.18E+05	2.22E+03

The data was then plotted with average area vs. sonication time and shown in Figure 23 below. Particle size had little change after 2 minutes of sonication, but on higher magnifications it was observed that there was an increase in the number of smaller particles with longer sonication times.

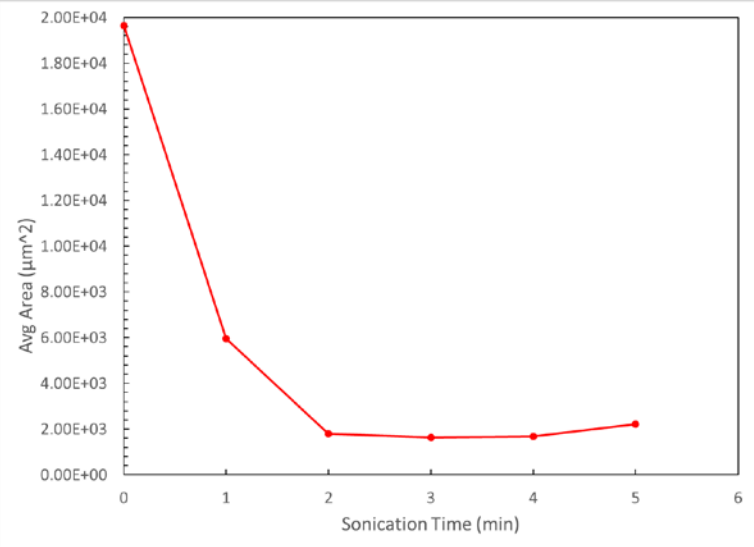

Figure 23: Plot of NGP agglomeration area with sonication time.

The particle analysis process works well at low magnification and to look at larger agglomerations. When the process is used with magnification images, the reflected light from the top lit microscope creates a bright area on the graphene/graphite particles. This lighter area on the particle is then converted to white in the binary image and excludes a large area of the particle. Figure 24 shows the binary images are shown with the original optical microscope images for both low and high magnifications.

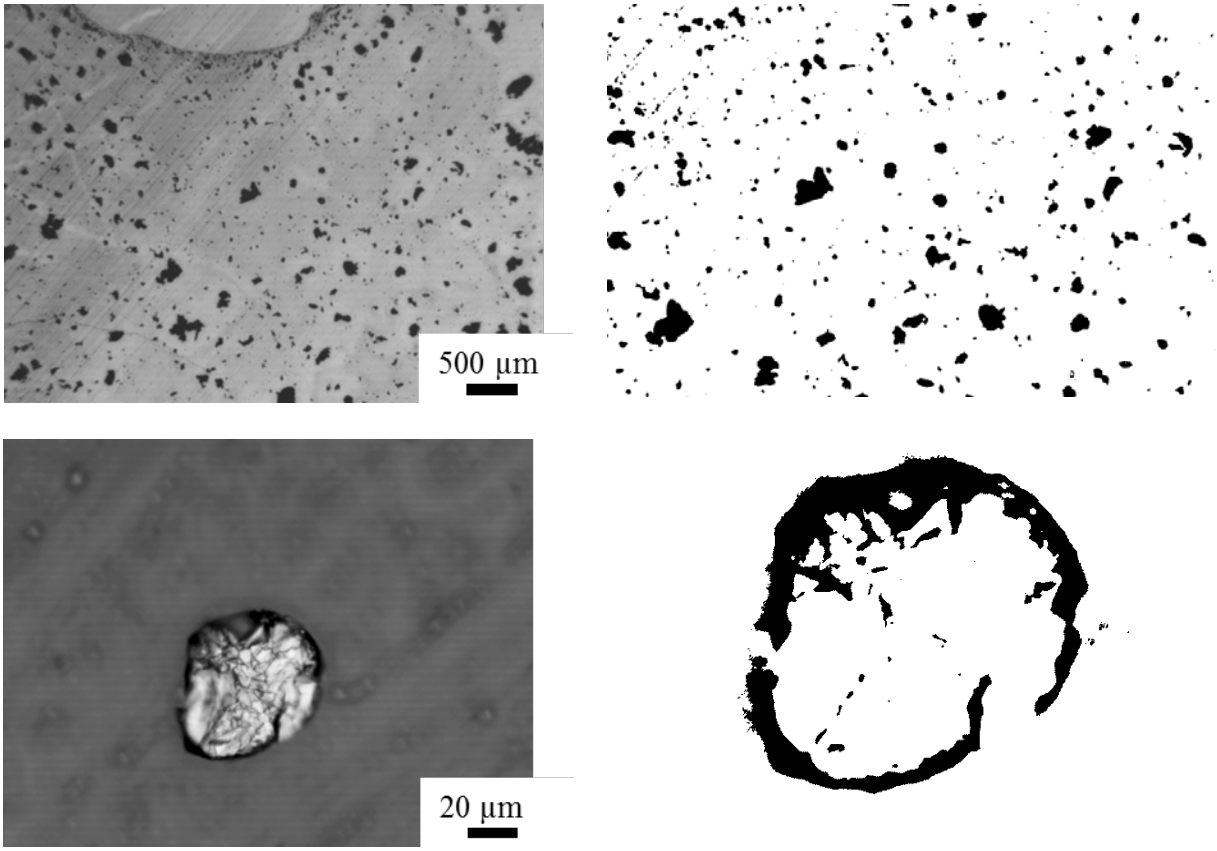

Figure 24: Top Left, low magnification (500 micron scale bar) image of NGP agglomerations. Top Right, binary image of low magnification NGP agglomeration. Bottom Left, high magnification (20 micron scale bar) image of graphite chunk. Bottom Right, binary image of high magnification showing reflected light converted to white space.

Samples of the NGP agglomerations were also prepared for scanning electron microscopy (SEM). The total sonication time was extended out to 10 minutes, and the NGPs were dispersed in acetone at a low concentration to prevent agglomeration.

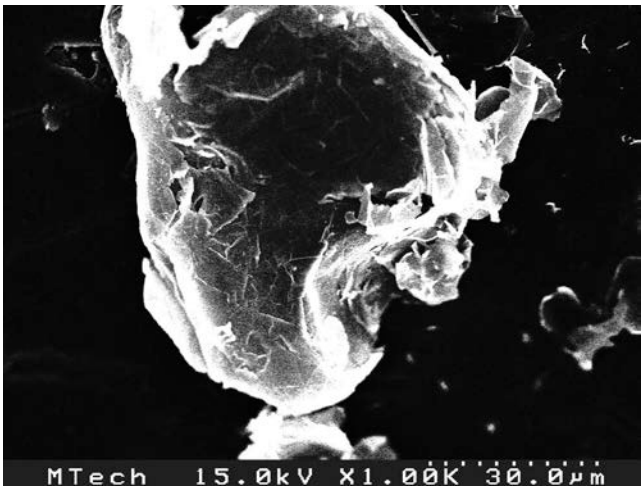

Figure 25: Graphite after 4 min of sonication.

Figure 25 shows a SEM image of a graphite particle after 4 minutes of sonication with dimensions of approximately 50 microns. After increased sonication time of 8 minutes, a NGP is shown in Figure 26 with a diameter of approximately 5 microns.

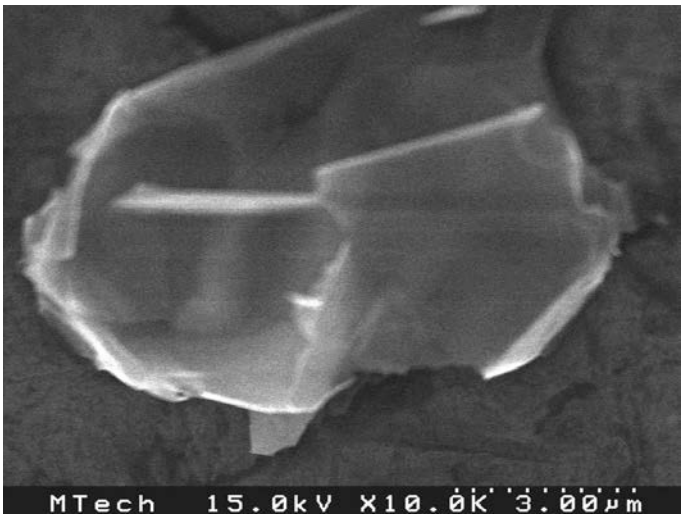

Figure 26: Graphene platelet after 8 min of sonication.

3.5.2. Bulk Graphene Resistivity Properties

To measure the electrical resistivity of the graphene a test fixture was created that would compress the graphene powder. Given the known dimensions of the cylinder and the thickness of the graphene disk, Equation (14) could be used to calculate resistivity.

$$R = \rho \frac{L}{A} \rightarrow \rho = \frac{RA}{L} \tag{14}$$

where R is the resistance of the fiber, ρ is the resistivity of the material, A is the cross sectional area, and L is the distance along the length of the fiber between the two voltage probes

An example of the setup is shown in Figure 27, with the measured dimensions of the cylinder the area, *A*, and length, *L*, known. The resistance was found from an I-V curve where the current was injected at the top of the graphene cylinder and removed at the bottom and a differential voltage was measured between the wires.

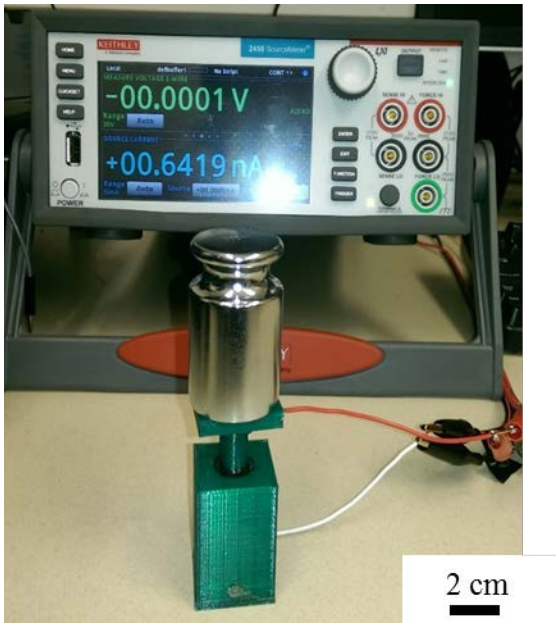

Figure 27: Test fixture setup for measuring the resistivity of the bulk graphene powder with a Keithley 2450 source meter, a weight was added to apply a constant pressure to the powdered graphene.

By having the voltage measured between the two wires suppling the current, as shown in Figure 28, the configuration is the same principle as the two-point probe discussed earlier. Since the measurement configuration is a two-point probe, the resistance that was measured was a total resistance which includes the resistance of the wires and the contact resistance made between the wire and the graphene. It was assumed that the wire resistance had a negligible impact on the current and voltage (I-V) measurements because of the short lengths of wire would contribute a negligible amount to the total resistance. Also, it was assumed that the test fixture would remain unchanged between testing each source NGPs, so that the wire and contact resistance would remain constant and only the material would vary.

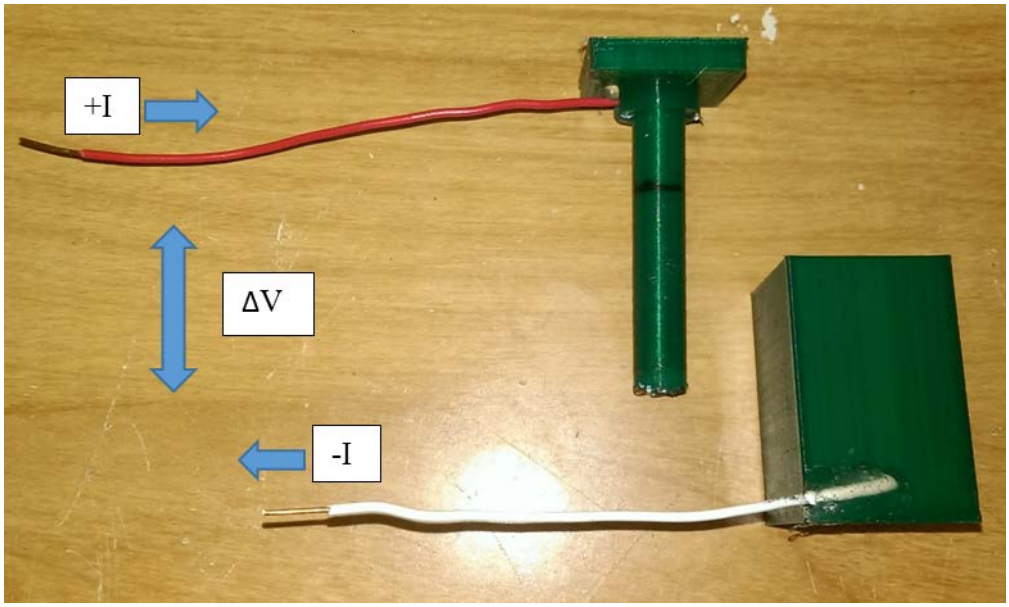

Figure 28: Current and voltage configuration for two-point probe I-V curve measurements.

Current and voltage data was collected on a Keithley 2450 source measurement unit and plotted, Figure 29. Current was swept from -5 mA to +5 mA for both samples of graphene, and

a slight change in the slope of the I-V curve was observed. The difference in the slope is caused by a change in the resistivity.

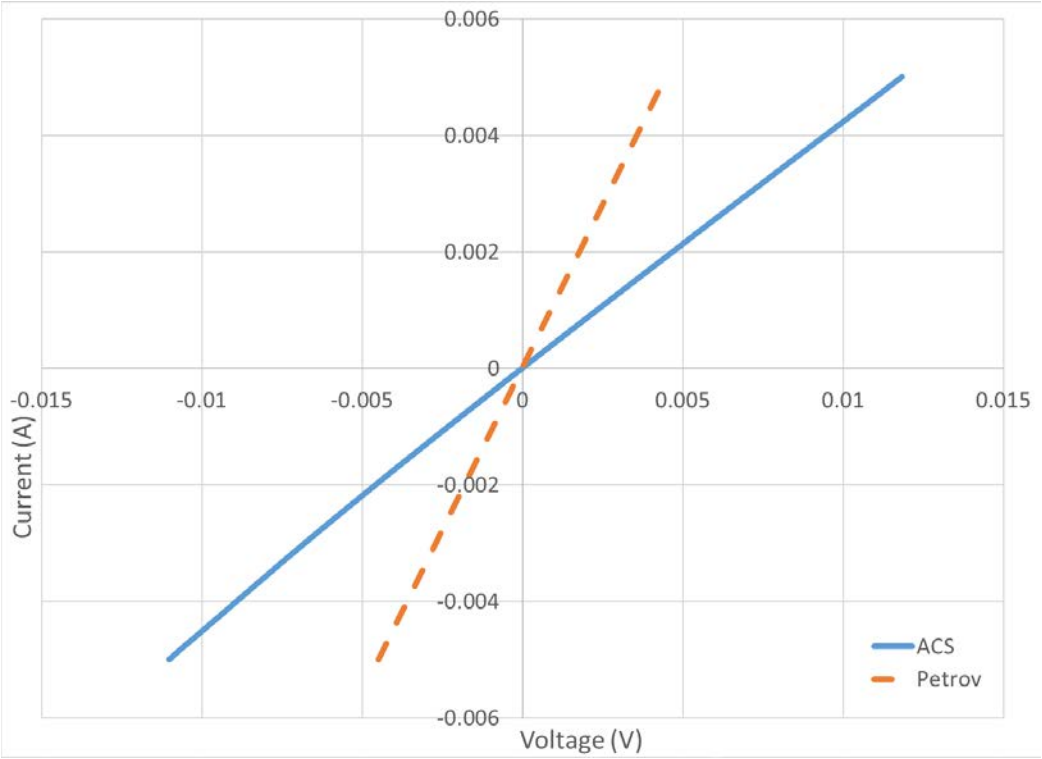

Figure 29: The measured current and voltage data from the powdered graphene samples demonstrated a linear I-V trend.

The linear trend of the I-V curves shows that the graphene has metallic electrical conduction properties. Also, the lack of any nonlinear regions suggests that the graphene and metal contacts are not making a semiconductor junction which is beneficial for future implementation. Then, by using equation (13) the resistivity was calculated and plotted as a function of voltage, shown in Figure 30 below.

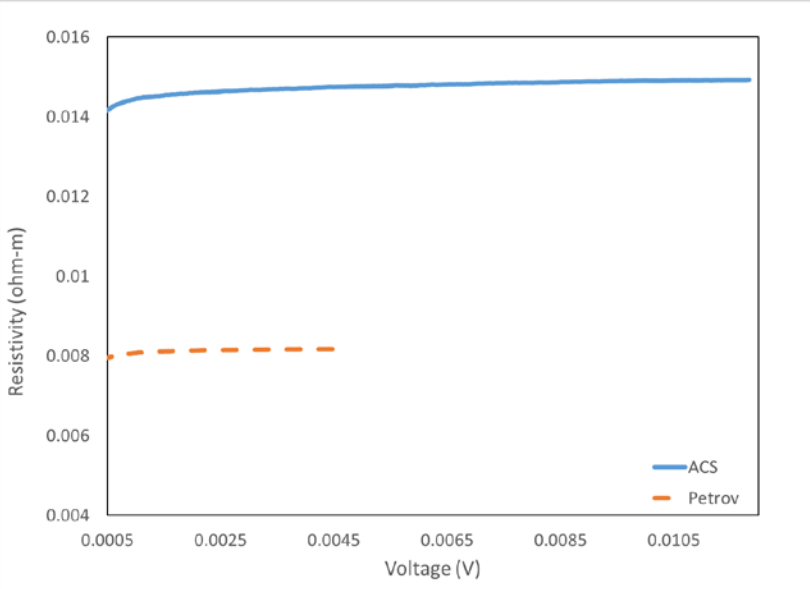

Figure 30: Resistivity plots of the new and old graphene showing constant resistivity values over the range of swept current and voltage.

Constant resistivity values also suggest that the NGPs have metallic electrical conductivity properties, which was expected because of graphene being a zero bandgap semiconductor material. Measured values were compared to the published values and shown in Table VIII below.

Table VIII: Resistivity values of the measured NGPs compared to the published values.

	Measured Value (ohm·cm)	Published Value (ohm·cm)
ACS Graphene	1.45	1.25x10^-3
Petrov Graphene	0.825	NA

The measured values were very different from the published value provided by ACS Materials. This could be due to the pressure used to compress the graphene, the contact resistance could have a larger impact than previously assumed, or the published value is a theoretical maximum for graphene. In either case the test fixture is useful for measuring resistivity trends.

3.6. Graphene Polymer Composite

3.6.1. Melt Mixing

The polymer stick mold was wrapped with a resistive heating element and connected to the melt electrospinner temperature control system. Then the mold was filled with polypropylene (PP) pellets, 14,000 MW amorphous, to determine an amount of pellets that would fit into the mold before melting. The pellets were weighed, the mass of the PP was 3.50 grams. For a 5wt% mixture of graphene, a mass of 0.175 grams was used and weighed in the fume hood. The graphene was added to the PP pellets in a sealed 50 ml plastic test tube. To mix the solid PP pellets and graphene, the mixture was sonicated at 50% power for 1 minute with the intent to break apart any large agglomerations. Then, the test tube was placed on the shaker for approximately 1 minute. Then the graphene coated PP pellets were poured into the heated mold and completely melted. A stirring spatula that had a width slightly smaller than the ½ inch diameter of the mold was used to increase shear mixing. Then, the mold was allowed to cool and form the solid PP/graphene stick shown in Figure 31, below.

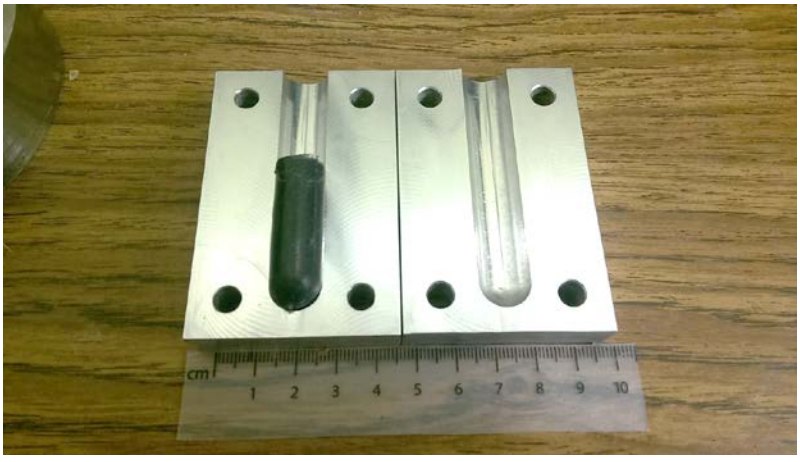

Figure 31: PP and graphene polymer composite cast into a stick to feed into the melt ES tool.

Last, to attempt to image the cross section and determine the amount of distribution, the stick was cleaved. The PP/graphene stick was placed on dry ice (~ -80^{o}C) below the glass

transition of PP (~-20^{o}C). After an hour it was snapped in half, and the cleaved surfaces were cut with a knife from the rest of the stick. The cleaved surface is shown in Figure 32.

Figure 32: Cleaved surface of the PP/graphene stick prepared to image the distribution of graphene throughout the cross section of the polymer stick.

The melt mixing step was improved by creating custom mixing tips, made from 12 AWG gauge steel wire, that fit into the chuck of a drill and used to mix the melted polymer in a metal crucible. Different shapes of the mixing tips are shown in Figure 33 below. High speed mechanical mixing appears to work well and achieves a fairly uniform distribution observed from optical micrographs.

Figure 33: Custom melt mixing tips for improved graphene dispersion. The shaft of the mixing tool was attached to the chuck of a handheld drill.

Resistivity measurements for the bulk PP/graphene composite (discussed later) showed conductivity with relatively high particle loadings. In order to reduce the particle loading and improve the dispersion of graphene within the polymer matrix, the melt mixing method was changed to a solution intercalation method.

3.6.2. Solution Intercalation Mixing

The solution intercalated mixing method was an attempt to reduce the viscosity of polymer composite to a point where the composite could be electrospun and reduce the fiber diameters. By dissolving a polymer in solution the NGPs could slip between polymer chains and create a intercalated mixture and improve dispersion while using less doping material. The solution intercalation method was performed with both 14,000 MW atactic PP and the recycled 220,000 MW general purpose PS. The semi-crystalline structure of PS allowed for the composite to be characterized by XRD, whereas, the PP has an amorphous polymer chain structure that would result in a poor XRD spectra.

A mixture of PS and graphene was made by dissolving the PS into solution, at ~20.0 wt%, with toluene. The graphene had been previously sonicated in acetone for 10 min and dried. The graphene was added to make a 1.0 wt% mixture in solution and just under 5.0 wt% (actual mixture was 4.5 wt%) once the toluene was removed.

3.6.3. XRD Characterization

Samples of the neat PS, graphene (or graphite) and PS/G mixture were prepared for powder XRD measurements. The XRD was setup to run a wide scan of 2ϴ angels from 5.0 to 90.0 degrees. After the data was collected, MATLAB was used to normalize and plot the XRD spectra for each component of the composite material. Figure 34 shows the PS XRD pattern that is primarily amorphous with some semi-crystalline structure.

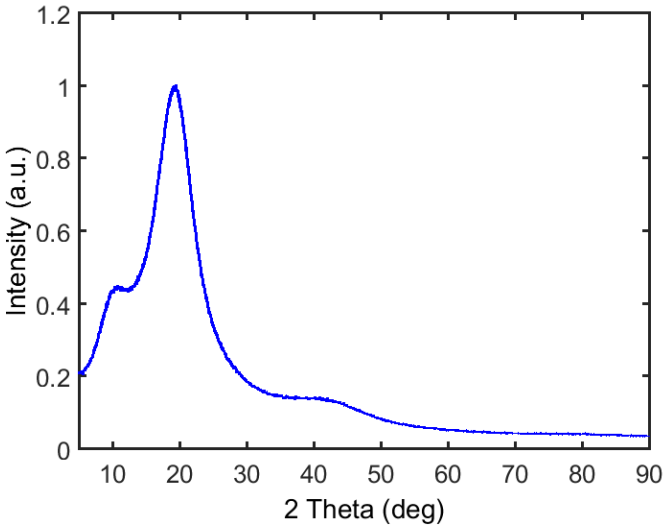

Figure 34: Powder XRD spectra of neat PS shows a broad peak typical of a semicrystalline polymer.

Figure 35 shows the graphite (001) peak at 26.44º 2ϴ, which was expected because of the large number of graphite crystals remaining with the NGPs.

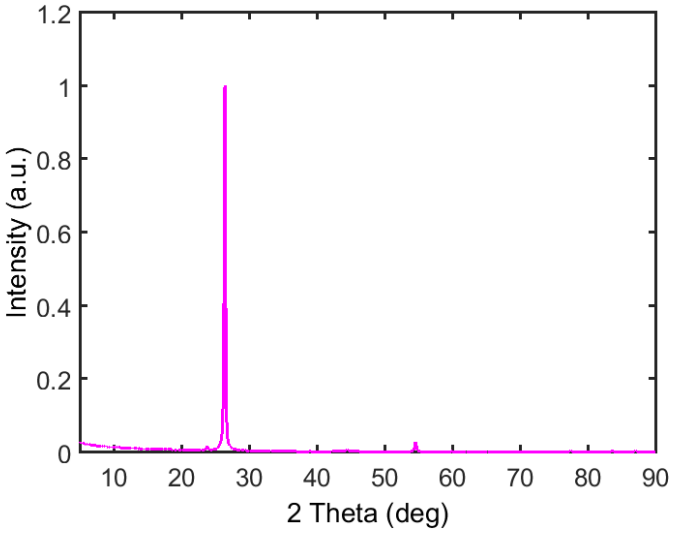

Figure 35: Powdered XRD spectra of NGPs and remaining graphite chunks.

Figure 36 shows the PS/G 4.5 wt% mixture XRD pattern which has a two phase XRD spectra. The two phase spectra is most likely because of the immiscible mixture of PS and graphite.

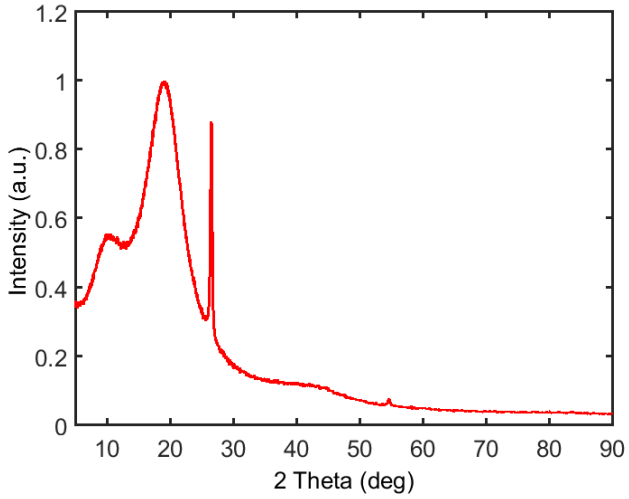

Figure 36: Powdered XRD spectra of the PS and NGP composite.

To compare the XRD spectra of the individual components and the XRD spectra of the composite, the curves were plotted together as shown in Figure 37, below.

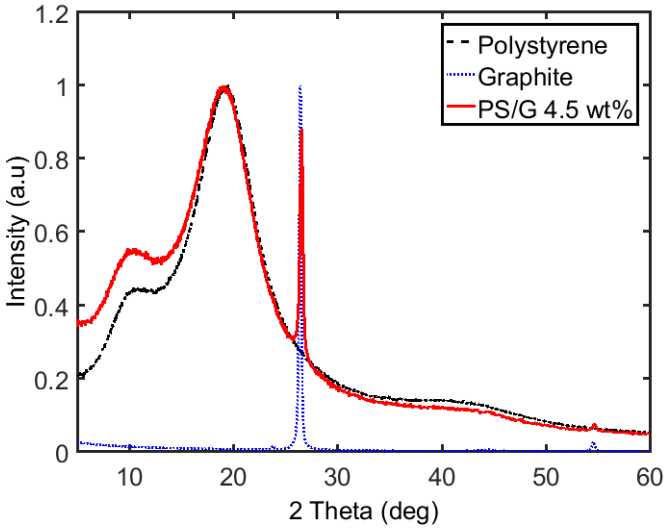

Figure 37: Powdered XRD spectra comparison to show slight peak shift from the intercalated mixture.

The slight shift in the amorphous PS peak at 19.5° to 19.0° 2Θ shows a slight increase in d-spacing of the semi-crystalline structure. NGPs create an intercalated mixture between the polymer chains causing the slight shift. The graphite (001) peak at 26.44° 2Θ in the PS/G mixture shows that the graphite creates an immiscible mixture with the PS.

3.7. Carbon Nano Tube Composite

CNT and polymer composite samples were prepared by Virginia Tech as a collaboration with SNL. The composite would be characterized and used to create conductive electrospun fibers at Montana Tech. The CNT/polymer composites had CNT loadings of 0.5 wt%, 1.0 wt%, 5.0 wt%, 7.5 wt%, and 10.0 wt% and used the 12,000 MW isotactic PP as the matrix material.

To determine the process temperature for the melt ES tool, the PP/CNT composite was heated to find an approximate melting point. A sample from each of the different loadings of CNTs was used to find an approximate melting point and viscosity. When melted the PP/CNT mixtures of 5.0 wt% and above were extremely viscous and retained the original shape. The temperature was raised, in attempt to decrease the melt viscosity, until the polymer began to

degrade. Table IX shows the recorded values from the melting point and the temperature where the composite began to degrade.

Table IX: Observed melting/soften points of the PP/CNT composite.

Mixture wt%	Melting point (°C)	Degrade (°C)
Neat	120	193
0.5	125	200
1.0	127	205
5.0	130	208
7.5	130	230
10.0	130	265

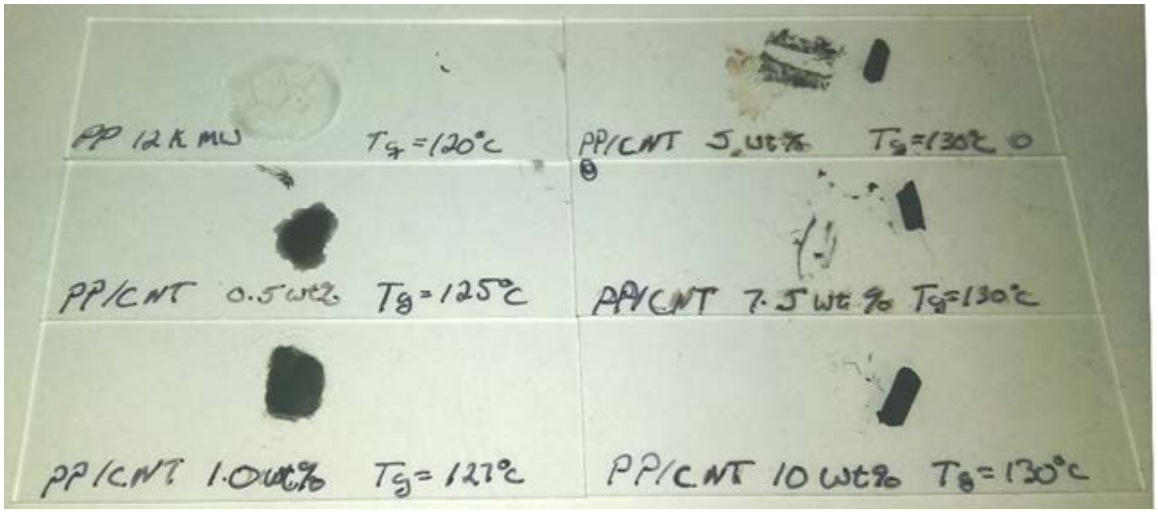

Figure 38: Melted CNT/PP composite to determine approx. melting point and viscosity for melt ES tool parameters.

Figure 38 shows the melted CNT/PP composite samples. For the CNT loadings of 5.0 wt% and above, the polymer would no longer naturally flow once it reached a temperature that the neat polymer would have become liquid.

3.8. Commercially Available Conductive Polymer Materials

Several companies have recently released conductive polymers for 3D printing applications. Proto-pasta makes a Conductive PLA printer filament which is made from Natureworks 4043D PLA, carbon black, and a proprietary dispersant. Resistivity of the

conductive PLA was measured with the same processes used for the graphene and CNT polymer composites. The following is a statement from the vendor describing how resistivity was measured:

> "We measured the conductivity using a fixture we machined that clamps a sample between 2 sheet conductors and 1cm cubes printed on a Printrbot Simple Metal and machined from solid resin."

To measure the volume resistivity the filament was melted onto a glass slide, and the resistivity was measured with a four-point probe. Table X shows the measured and published values for the resistivity of the conductive PLA filament.

Table X: Measured vs published values for the conductive PLA filament.

	Measured Value (ohm-cm)	Published Value (ohm-cm)
Volume Resistivity	270	15
Fiber Resistivity	35.4	3.8

Values shown in Table X are best used as a comparison to other resistivity values measured for the graphene and CNT composites because of the similar methods used to measure resistivity. The published values have a different method and appear to have significantly different results.

3.9. Composite Electrical Properties

The electrical resistivity of the composite materials was characterized by four-point probe measurements. Also, the resistivity measurements were checked by using the van der Pauw method. Figure 39 shows an example of the glass slides that were produced with each set of polymer composites. On the left is a coverslip that was used to spread the melted composite into a thin film so that the dispersion and particle size could be observed. In the center is a van der

Pauw Greek cross structure. The Greek cross structure was created by 3D printing a PLA polymer mold and then filled with solid composite material and heated until melting. The mold material was chosen so that it had a higher melting point than the composite. Because of the different melting points in the polymers, there was a distinct boundary between the mold material and the composite. The Greek cross structure was then attached to the slide with nail polish. On the right is a four-point probe thick film sample where the composite was melted and spread into a film less than 1.0 mm thick. By keeping the film thickness between 0.5 mm and 1.0 mm then Equation (5) for calculating resistivity was still valid.

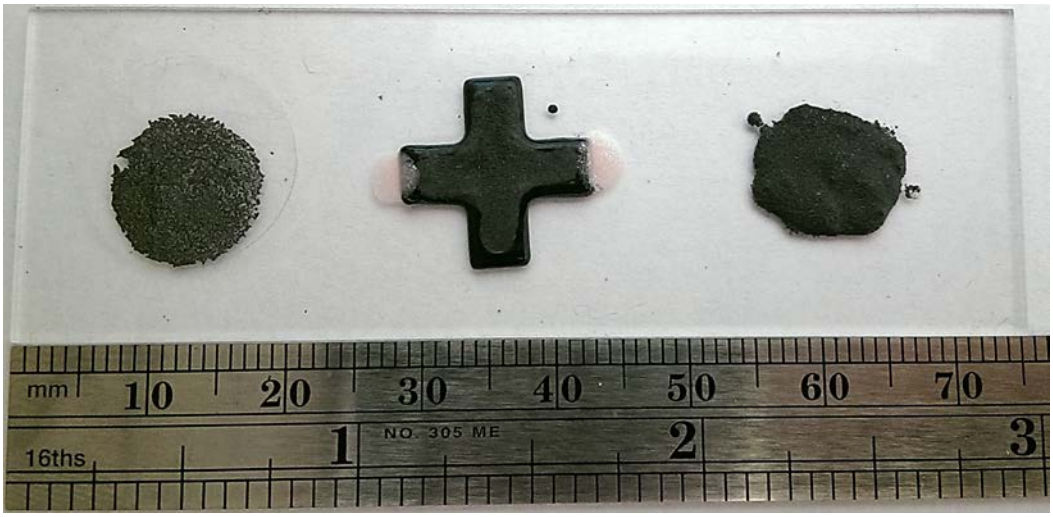

Figure 39: Example of glass slide used to characterize composite electrical properties. Left, cover slip with composite thin film. Center, van der Pauw Greek cross structure. Right, four-point probe thick film sample.

3.9.1. Four-Point Probe vs van der Pauw Resistivity Calculations

Some of the first four point probe measurements were made with the PP and CNT composite from Virginia Tech. The Polypropylene and Carbon Nanotube (PP/CNT) mixtures were at 0.5 wt% , 1.0 wt%, 5.0 wt%, 7.5 wt%, and 10.0 wt%. The plot of the I-V curve is shown in Figure 40 below to compare the changing weight percent of CNT loadings.

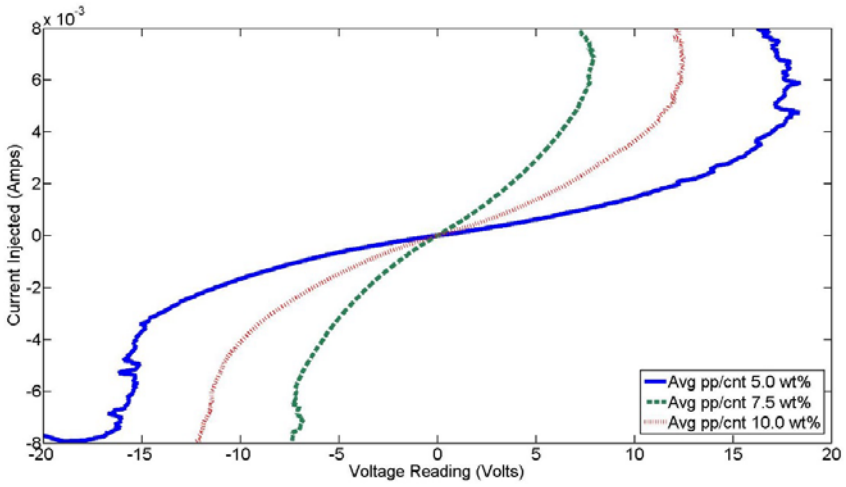

Figure 40: I-V curve of the Virginia Tech PP and CNT composite.

Since, the mixtures of 0.5 wt% and 1.0 wt% were too low of concentration of CNT to be conductive I-V curves were not recorded. Results for the 10.0 wt % loadings were not expected, with a higher concentration of CNT's it was predicted that the resistance would decrease. Instead, the highest concentration had a greater resistance. The materials with the least resistance was the materials in the middle of the range of mixtures. Resistivity was then calculated and plotted against the voltage as shown in Figure 41 below.

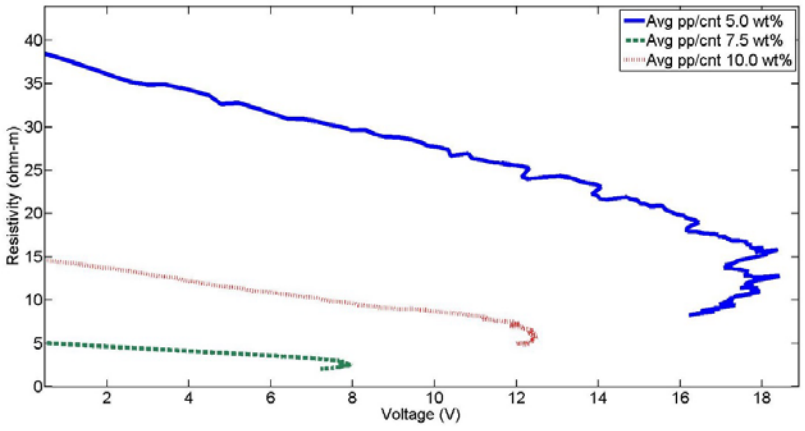

Figure 41: Resistivity plot of the Virginia Tech PP and CNT composite.

To test the accuracy of the four-point probe method the van der Pauw method was used as a redundancy with the same PP/CNT composites. A comparison of the calculated resistivity values is shown in Table XI below.

Table XI: Comparison of calculated resistivity values by four-point probe and van der Pauw methods.

Weight Percent (wt%)	Four-point probe Resistivity (Ω·m)	Van der Pauw Resistivity (Ω·m)	Percent Difference
5.0	13.23	13.83	2.2%
7.5	3.13	5.30	25.7%
10.0	7.20	8.85	10.3%

Results from the four-point probe and van der Pauw resistivity values produced similar values and provided confidence in the testing procedure. The four-point probe method is the simpler method and was implemented the most while the van der Pauw was used as a redundancy.

3.10. Variations in NGP Effect on Composite Resistivity

The two sources of NGPs discussed earlier had significantly different electrical resistivities and material properties. Once the NGPs were added to the polymer matrix, the different resistivity values had a similar effect on the composite resistivity. The I-V curve is shown below in Figure 42.

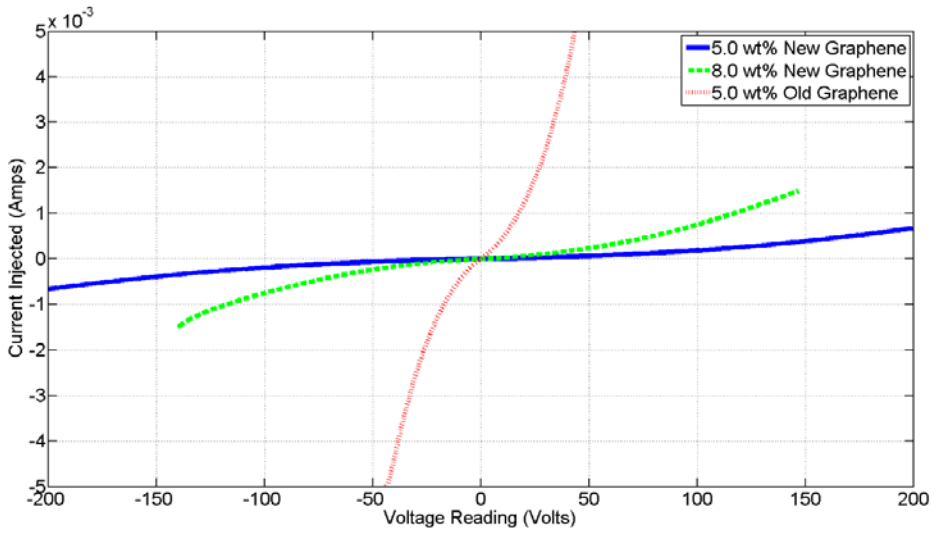

Figure 42: I-V curve comparing "old" Petrov supplied NGP and "new" ACS supplied NGP properties.

The significantly higher resistivity of the ACS NGPs is shown in Figure 43 when compared to the Petrov NGPs in the same 5.0 wt% loadings. Also, Figure 43 shows that increasing the particle loading of the ACS NGPs to 8.0 wt% had minimal effect in achieving a resistivity value similar to that of the Petrov NGP composite resistivity.

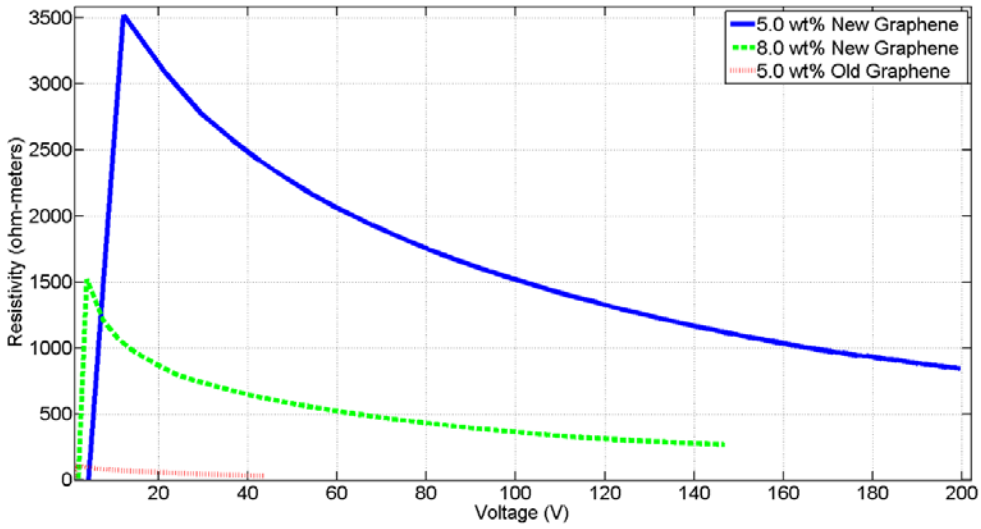

Figure 43: Resistivity of "old" Petrov NGP composite and "new" ACS NGP composite.

The resistivity plot shows that the mixtures of PP with the “new” ACS NGP composite resistivity is on the order of 1,000’s of ohm-m whereas the previous mixtures of PP and Petrov NGP composite were on the order of 10’s of ohm·m. To reduce the resistivity of the composite made from the NGPs supplied by ACS Materials, further processing would be required. The processing techniques that would be used include: graphene processing using sonication to exfoliate and dispersion improvements using solution intercalation mixing.

3.10.1. Effect of Sonication

The first study evaluated the effect of ultrasonic processing of the graphene on the electrical properties in the composite. Two composites of PP and graphene were created by melt mixing at a constant 8.0 wt% particle loading. The first graphene and polymer composite made from the ACS Materials NGP was not changed from the supplied form. In the second composite mixture, the NGPs were sonicated in acetone at a power of 450 W for 2.0 minutes and then dried before adding to the polymer melt.

The bulk material was tested for its resistivity properties using the four-point probe method. Figure 44 shows the I-V plot of the two 8.0 wt% samples without and with sonication. The resitivity was then calculated and is shown in Figure 45 below.

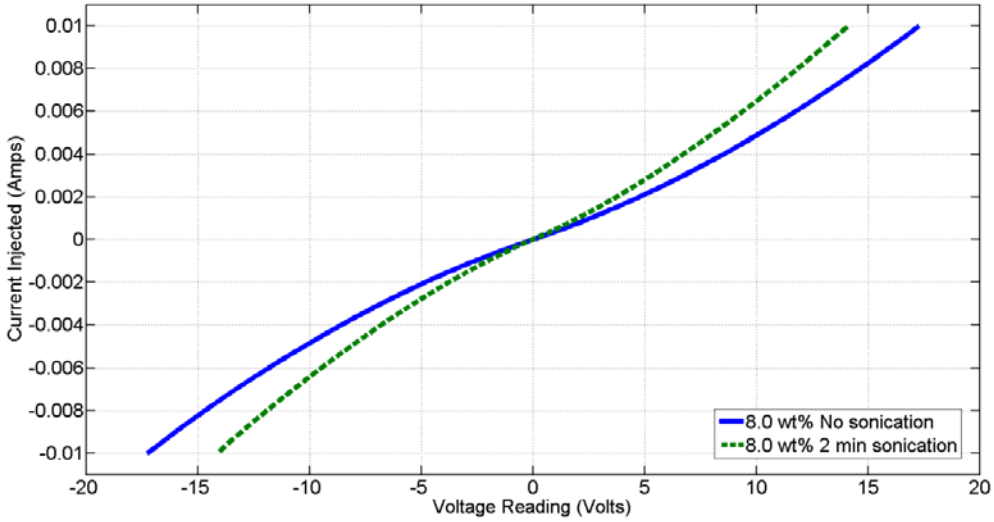

Figure 44: I-V curve showing the effect of ultrasonic processing on electrical properties of ACS supplied NGP in PP composite.

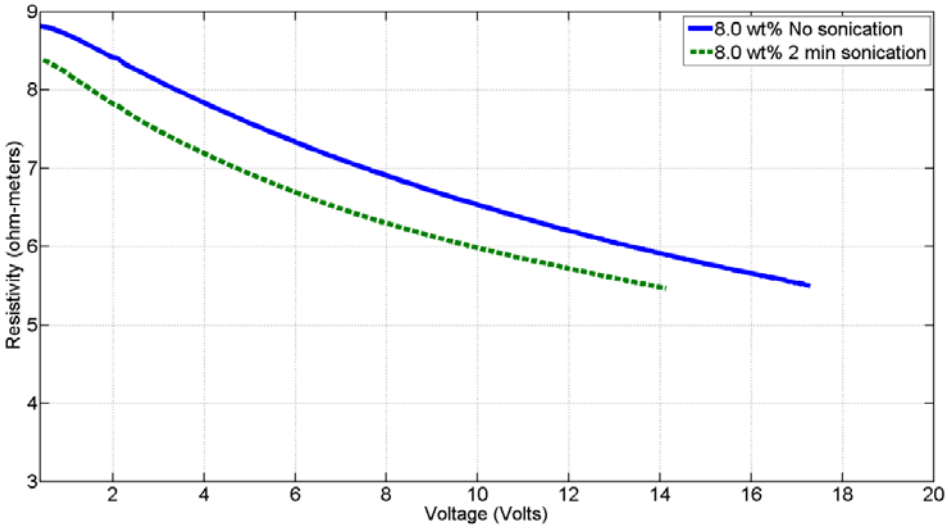

Figure 45: Resistivity curve showing the effect of ultrasonic processing on electrical properties of ACS supplied NGP in PP composite.

As expected the resistivity of the composite made with ultrasonic processed NGPs decreased because of the smaller graphene agglomerations. The next step was to create an optimized composite based on increased sonication time.

3.10.2. Effect of Melt vs Solution Mixing

The next study evaluated the effect of mixing methods on the electrical properties in the composite. Two composites were made with ACS Material supplied NGPs in the as received form and used the 14,000 MW atactic PP as the matrix material. The first composite was made by the melt mixing process at a particle loading of 5.0wt%. The second composite was made by dissolving PP into toluene, and the NGPs were added to the solution at a particle loading of 5wt% and then allowed to dry by evaporating the solvent.

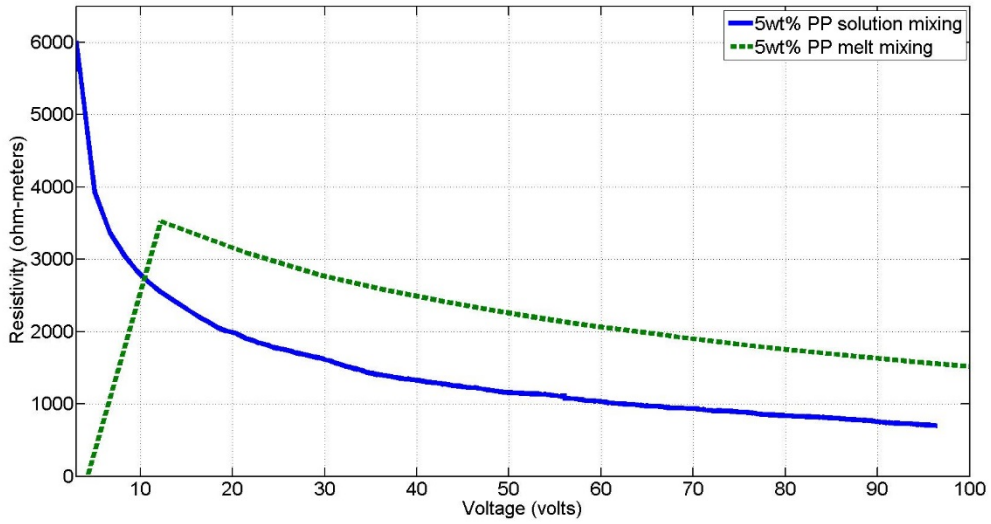

Figure 46: Resistivity plot showing the effect of solution intercalation mixing and melt mixing on the composite.

Figure 46 shows the results from the four-point probe measurements when the composite was made by melt mixing and solution intercalation mixing methods. The improved dispersion of the intercalated mixture helped to decrease the resistivity of the composite material. For the optimized graphene composite, the solution intercalation method will be used to help improve dispersion while using a lower particle loading.

3.11. Fiber Electrical Properties

Melt electrospun fibers from a 4.5 wt% loading of PP/NGPs was used to first test the DC resistivity. The melt ES fibers had a fiber diameter ranging from 300 microns to 600 microns, which was large when compared to most melt electrospun fibers on the order of 10's of microns. Resistivity was measure with the far-field probe station micromanipulator tungsten probes. Tungsten probes were placed collinearly along the length of the fiber and the spacing was recorded. Four micromanipulators were connected to the Keithley 2450 source measure unit to take a four-point probe measurement. Figure 47 shows the far-field probing station and the Keithley 2450 source measure unit setup for measuring fiber conductivity.

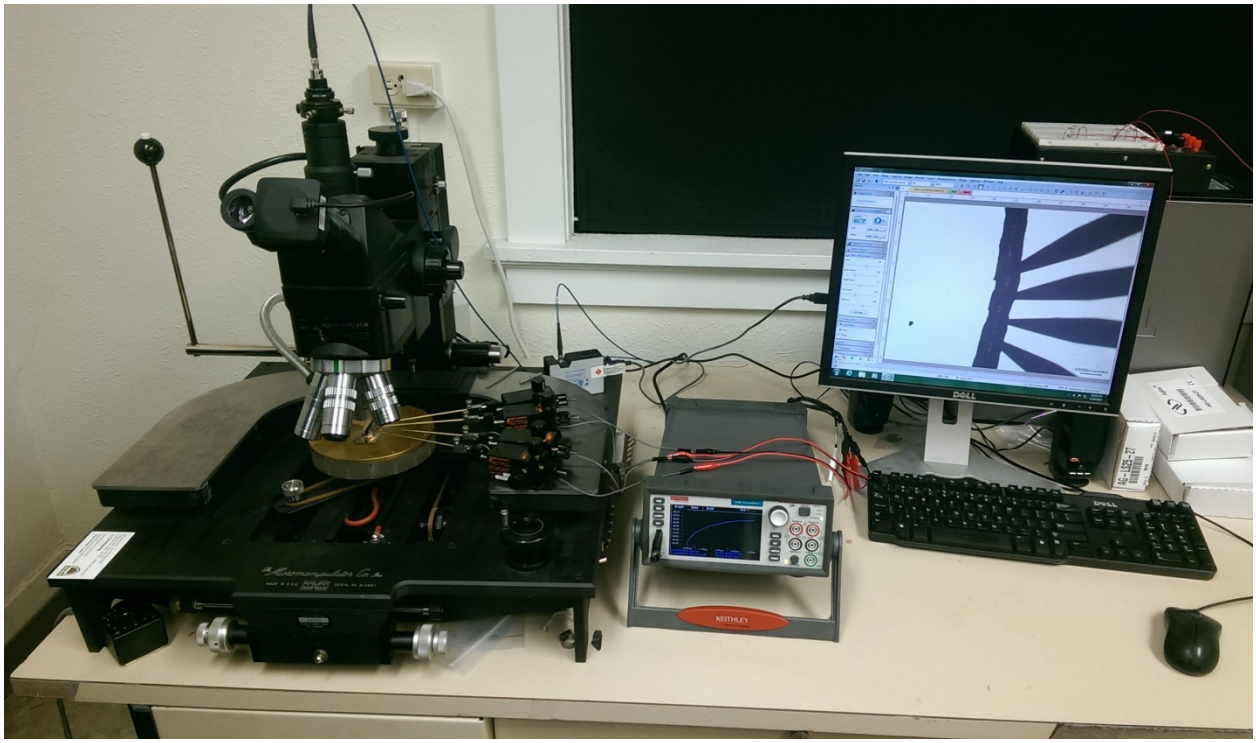

Figure 47: Far-field probing station with micromanipulator tungsten probes for current and voltage measurements with Keithley 2450 source meter.

Figure 48 shows a close up view of the micromanipulators and the four tungsten probes setup in a collinear configuration underneath the microscope objectives.

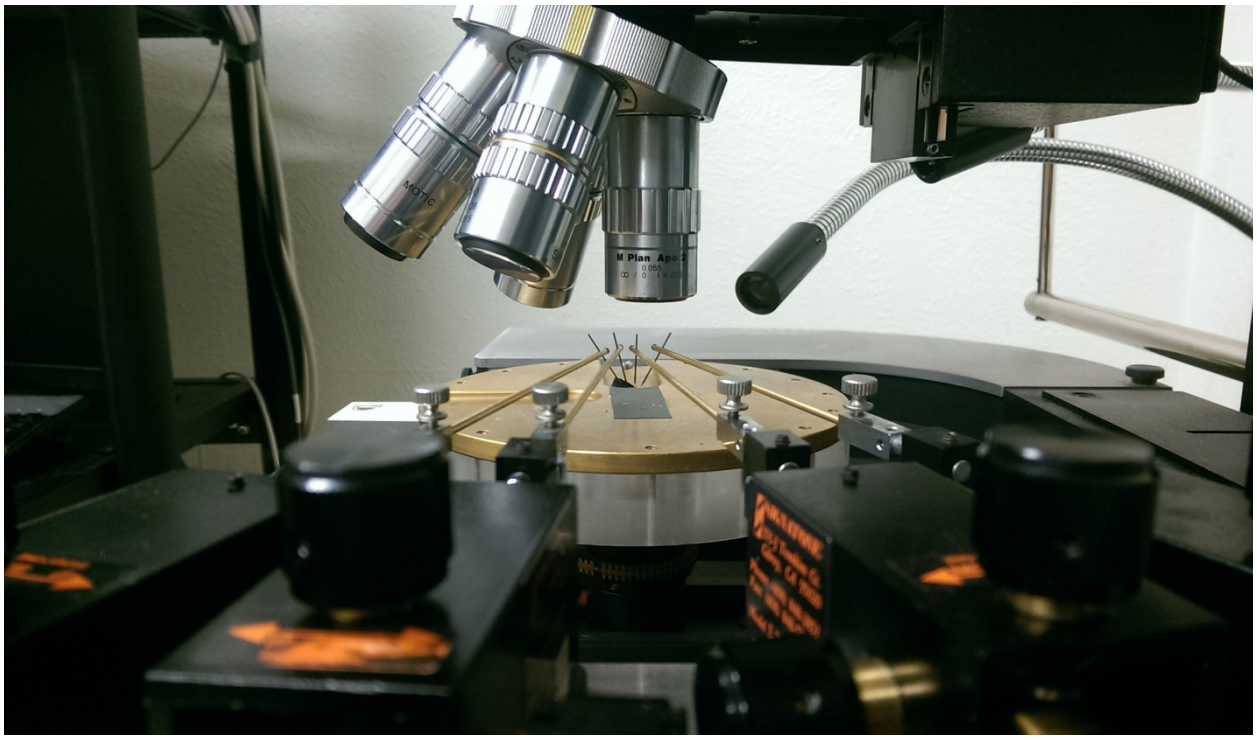

Figure 48: Micromanipulators and tungsten probes arranged in a collinear configuration for four-point probe resistivity measurements.

The outside current probes were landed onto the fiber first in attempt to pin the fiber in place before the center two voltage probes were landed. To land the probe the microscope objective was moved independent of the stage and micromanipulators so that a higher magnification view of the probe landing could be observed. The microscope focus was set slightly above the surface of the fiber and then the probe was lowered down into view. Focus was then adjusted again to the surface of the fiber and the probe was lowered the rest of the way until it made contact. The microscope objective was then repositioned at the next probe and the steps were repeated until all four probes were making good contact. A low magnification image of the probes is shown in Figure 49, with a probe spacing of 0.5 mm.

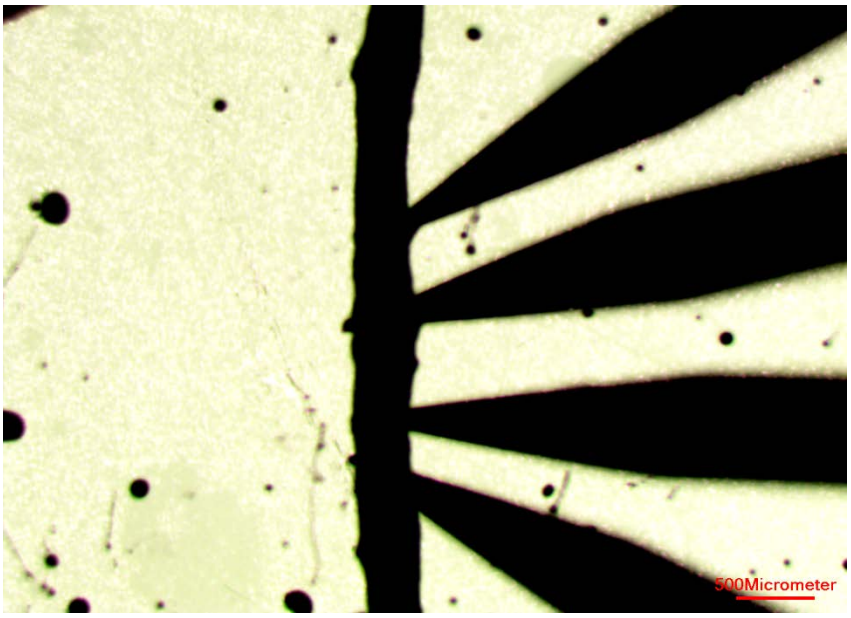

Figure 49: Optical microscope image of collinear tungsten probes on an electrospun fiber with 0.5 mm probe spacing.

Multiple fiber diameters (320, 420, 620 microns) were measured and then the resistivity was calculated and plotted. The I-V curve is shown in Figure 50 and the calculated resistivity plot is shown in Figure 51 below.

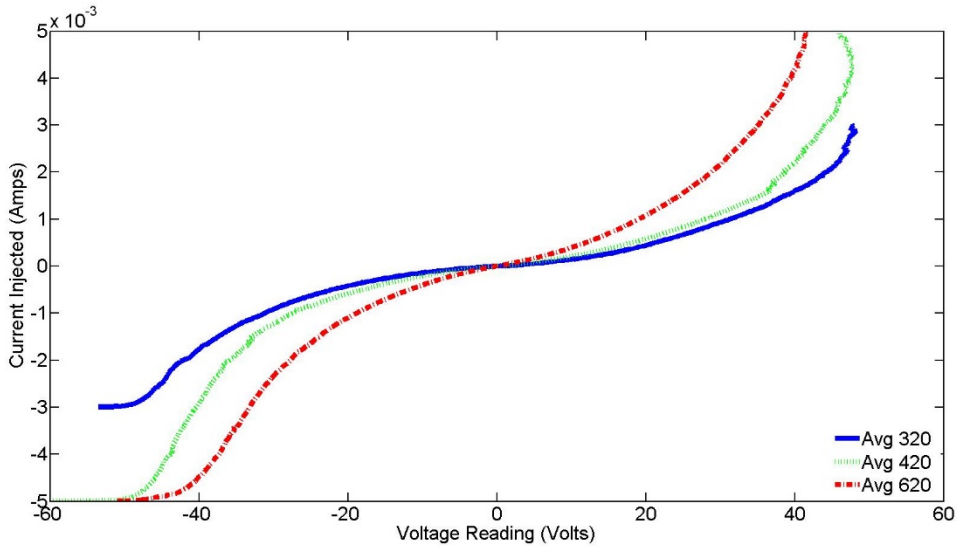

Figure 50: I-V curve data for multiple fiber diameters measured with the micromanipulator collinear probes.

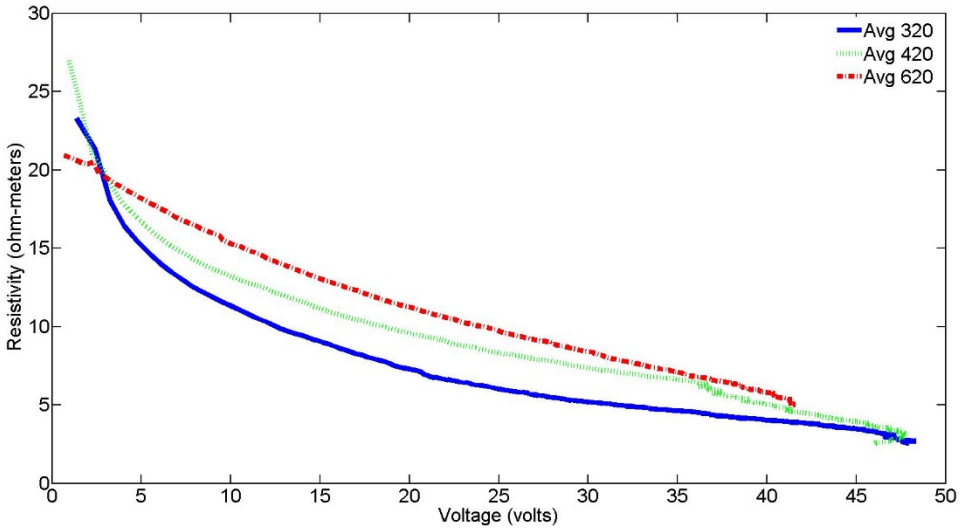

Figure 51: Resistivity plot of multiple fiber diameters measured with the micromanipulator collinear probes.

Calculated resistivity appears to have a large variation for different fiber diameters. Resistivity was expected to be nearly constant for each fiber because all of the fibers were made from the same material and resistivity is an inherent material property. The difference in resistivity is most likely caused by two factors. First, the change in cross sectional area of the fiber allows for more current to flow through the fiber. Second, the resistivity could be affected by the way that the agglomerations of graphene are distributed throughout the polymer.

3.12. Optimizing Material Conductivity

The techniques that resulted in the best conductivity (solution intercalation mixing and sonication) were combined to make a composite that was optimized for the lowest resistivity. A composite was made with a 6.0 wt% particle loading in the 14,000 MW atactic PP matrix. Graphene was added to the polymer and toluene solution and then sonicated for 1.0 minute

intervals and repeated for up to 4.0 minutes. After the appropriate sonication time, the solution was drop casted into a thin film and allowed to dry.

The agglomeration of graphene was imaged using an optical microscope. The images in Figure 52 below show the size of the agglomerations as well as the general dispersion of the graphene within the polymer when spread into a thin film under a coverslip. Images A-E are taken from samples with no sonication up to 4 minutes of sonication respectively and show an apparent increase in smaller graphene particles throughout the polymer.

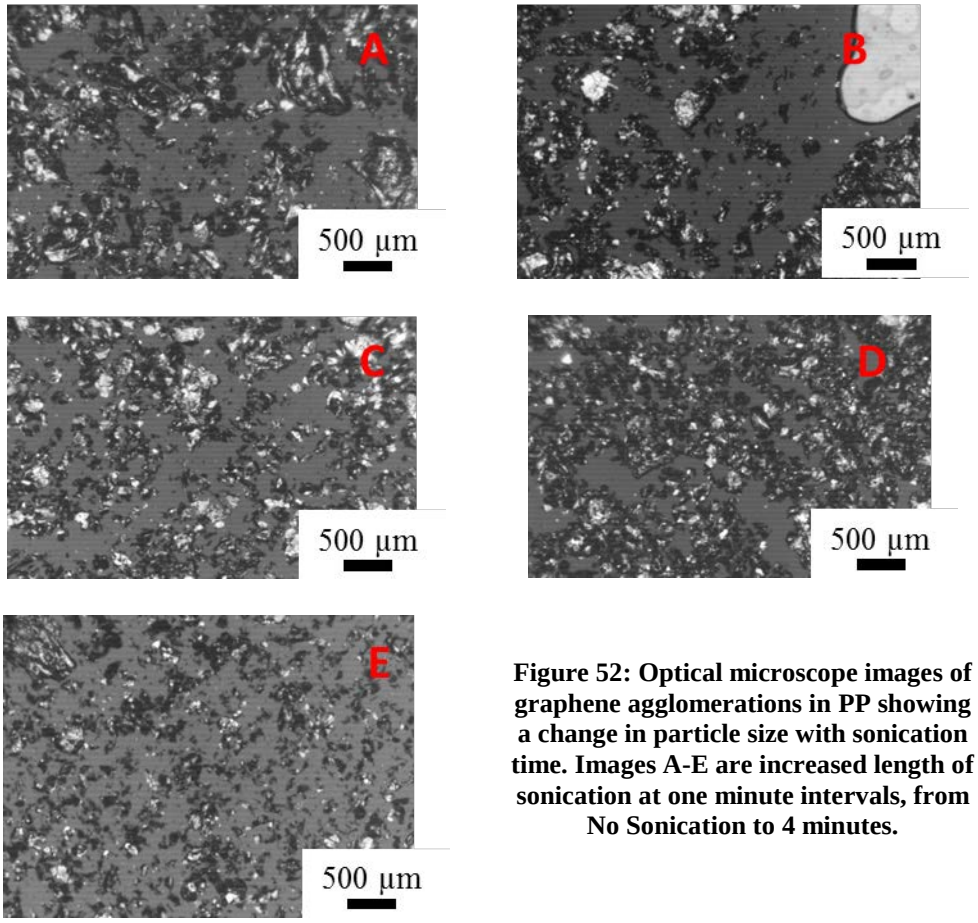

Figure 52: Optical microscope images of graphene agglomerations in PP showing a change in particle size with sonication time. Images A-E are increased length of sonication at one minute intervals, from No Sonication to 4 minutes.

Using ImageJ these images were analyzed using a black and white threshold to generate a binary image, then the particles could be counted and measured. These values are shown in Table XII below.

Table XII: Particle count and size after ultrasonic processing.

Time (min)	Count	Avg.Size (µm^2)
0	624	150.3
1	583	105.7
2	773	100.7
3	1808	65.0
4	1724	42.2

DC electrical properties of the PP/G composite were measured with a four-point probe. The I-V data for each length of sonication time was averaged with multiple data sets and then plotted. This is shown on the left in Figure 53 below. The average of the data sets was then used to extract a resistivity for each length of sonication time, shown on the right in Figure 53.

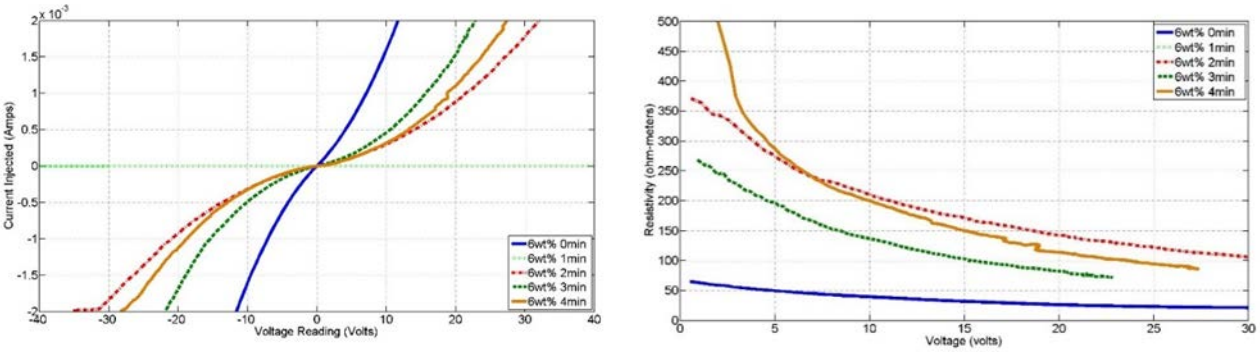

Figure 53: DC Electrical measurements of the bulk PP/G composite at 6wt% graphene. Left, I-V curve generated from four-point probe measurements. Right, calculated resistivity values from I-V curve data. The resistivity data for 1 minute of sonication could not be plotted but had a value of approximately $1x10^6$ ohm-meters.

The slope of the line in the I-V curve represents the inverse of resistance, which is also proportional to the conductivity of the material. Mixtures that were not sonicated show the lowest resistivity and this was expected because of the largest agglomerations of graphene. These large agglomerations allow for multiple conductive pathways to be created with minimal number of junctions between agglomerations; this property would be beneficial for creating the

most conductive material. These large agglomerations pose a problem when the material is used to create ES fibers that are smaller than the agglomerations. After sonication the resistivity plot shows a trend that there is an optimal particle size created after 3 minutes of sonication. As the graphene agglomerations are broken up into smaller particles the resistivity decreases. With further sonication the particle does not become smaller but there is an increase in the number of particles. This increase in particles means that the number of junctions between the graphene also increases, causing the increase in resistivity.

3.12.1. Fiber Conductivity

The increased viscosity from the addition of the graphene has greatly increased the fiber diameter. Previously, fibers without graphene have been created on the order of 50 microns using the same melt ES tool and polymer. The melt ES tool had a 17 gauge hypodermic needle with an inside diameter of 1.067 mm and an applied voltage of 16 kV. The separation distance was 3.0 cm and the mid-plane collector was positioned in the middle at 1.5 cm from the needle. The electrospun fibers that were produced ranged from approximately 300 microns up to 600 microns.

Current and voltage data was measured for the fibers by using four micromanipulator probes placed along the length of the fiber. From the recorded I-V data the resistivity could be calculated. The resistivity plot in Figure 54 shows that for a constant fiber diameter of 510 μm +/-10 μm there is a decrease in resistivity with the sonication time. The data from the mixtures with no sonication and 1 minute of sonication were excluded because of the large agglomeration size that is not practical for future work of reducing the fiber diameter.

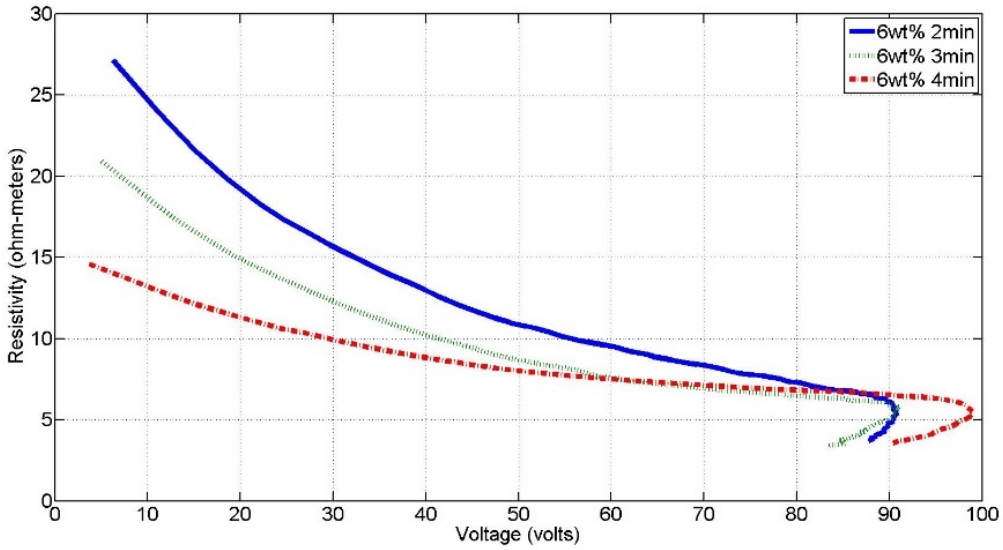

Figure 54: Calculated resistivity values for a constant fiber diameter of ~500 microns.

The trend of deceasing resistivity shown in the plot would suggest that the melt ES process has an effect on the packing or rearranging of the graphene particles. There was a significant decrease in resistivity when comparing the bulk material to the electrospun fibers. The resistivity of the fibers are an order of magnitude less than the bulk material. Also, the polymer composite fibers do not appear to be influenced by the number junctions between graphene agglomerations because of the decreasing resistivity with longer sonication times. There is no longer an optimal particle size that corresponds to the 3 minutes of sonication as observed in the bulk composite.

3.13. Filament Extruder Modifications

Future work with the melt electrospinning will include utilizing the motion control from a 3D printer to direct the deposition of the fibers. In order to adapt a 3D printer, the printer also needs to work with materials that are capable of being electrospun. The Filabot Original filament extruder was purchased and some modifications were made so that filament could be made from materials not intended to be 3D printed. The modifications to the Filabot Original included a

motor speed controller, convective cooling fans, filter, and larger nozzle size for working with PET.

Pulse Width Modulation (PWM) control uses high speed switching to turn the motor on and off from 0.0 V to 24.0 V and the motor speed changes by varying the duty cycle. PWM was used so that the motor would operate at its maximum torque specification. If the voltage supplied to the motor was controlled, the motor would operate at a lower torque. The Filabot Original has a 24.0 V DC motor that draws 3.0 Amps, the motor controller was rated for 6.0V to 90.0 V and 15.0 Amps. This motor speed controller was installed with the existing switch to cut power to the device and motor.

A cooling fan was placed ~ 2.0 in from the extruder nozzle with the air flow forced upward. The fiber was then supported and directed through the air column while it continued to extrude. When the fan was placed closer to the nozzle, the temperature dropped low enough for the PET to solidify and stop extrusion.

A 40 mesh (400 µm) sieve screen was installed to filter the melted polymer flow and The extruder nozzle was drilled out to 1/16 in (1.59 mm) from its original diameter of 1.3 mm. The 400 µm screen appears to remove the majority of the paper and has not affected the flow of polymer melt.

3.13.1. Process Parameters

The process parameters that provide the best filament with the modified Filabot are shown in Table XIII. Auger speed varied depending on the temperature of the nozzle which effects the viscosity of the extruded polymer. At full speed the auger will turn at 35 RPM.

Table XIII: Filament Extruder process parameters for recycled PET.

Temperature Controller Set Point	253º C
Nozzle Temperature without cooling	230º C
Nozzle Temperature with cooling	180º C
Auger Speed	10-20 RPM
Filament Diameter	1.52 mm – 1.77 mm

Figure 55 shows the effect of changing the location of the fan to help quench the PET in an amorphous microstructure. On the left the air column from the fan is ~2.0 inches from the nozzle and the filament was translucent, which might indicate that the majority of the microstructure is amorphous. On the right the fan was placed further away, and less air was directed upward. This configuration resulted in opaque and brittle filament most likely because of a semi-crystalline microstructure.

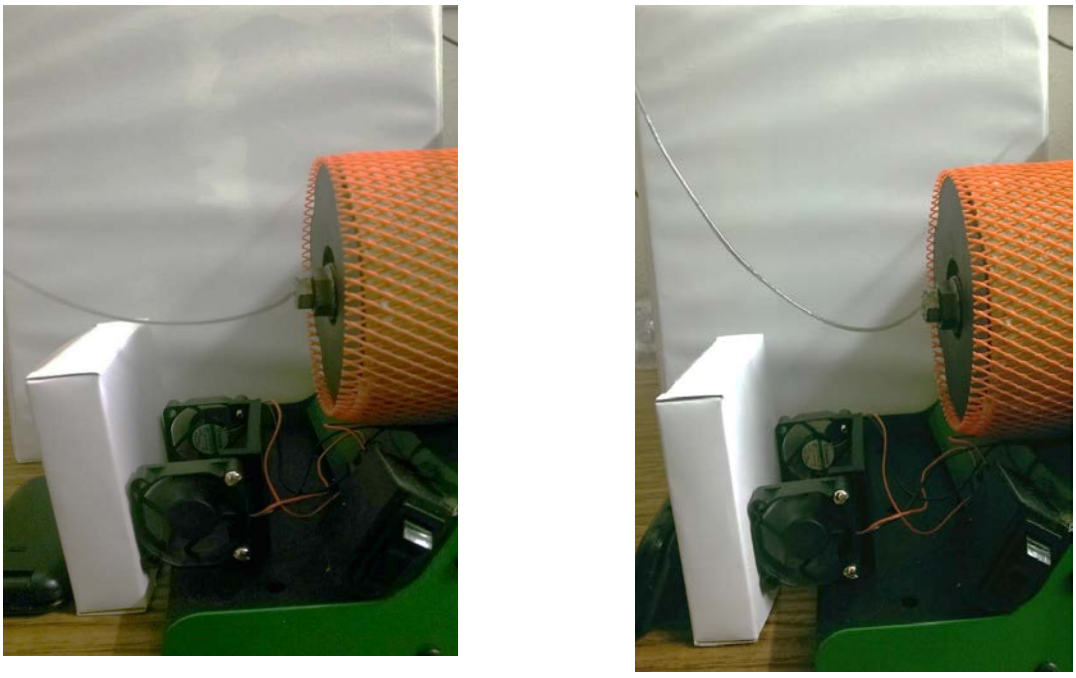

Figure 55: Convective cooling fan placement effecting the crystallization of the recycled PET filament.

Figure 56 shows the first few layer of a test print from a short length of the 2.4 mm filament in the LulzBot Taz 5 using T-Glase PETT print settings with the temperature raised to

255^{o} C. This was from the initial filament before the filter was installed and there were a few problems with clogging. On the left is a standard PLA print for comparison.

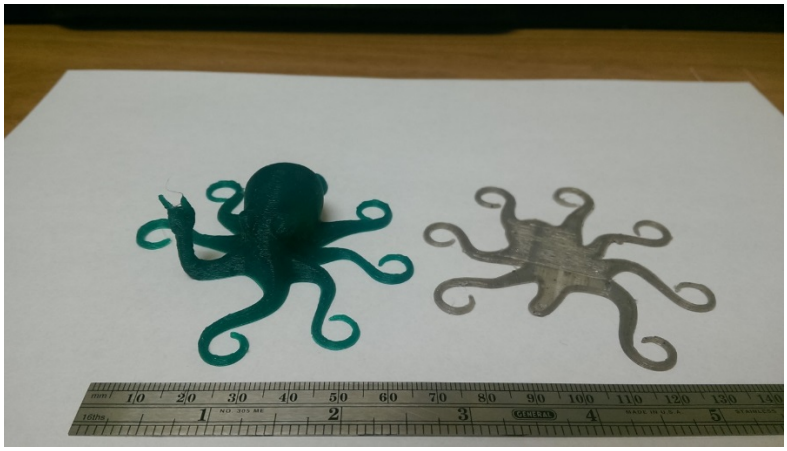

Figure 56: First few layers of recycled PET test print compared to a standard test print with PLA.

4. Discussion of Results

4.1. Material Processing

The NGP material obtained from ACS Materials consisted mostly of graphite powder with large agglomerations of NGPs. Initial tests with low particle loading from the raw material resulted in poor performance for the materials ability to be electrospun and the electrical conductivity. Material obtained from ACS Materials would require additional processing to meet the requirements of this project. Several methods of creating exfoliated graphene from graphite powder were considered, such as thermal or chemical exfoliation. Ultrasonic processing was the simplest and most flexible option for the small quantities used in creating each batch of composite material. The ultrasonic processing showed an order of magnitude change in particle area after 2.0 minutes. When observed with higher magnification the particles continued to decrease in size until they reached the dimensions reported by the manufacture of approximately 5.0 microns. ImageJ particle analysis proved to be a useful tool for measuring and counting the graphite/graphene agglomerations. The best results were achieved by using a lower magnification so that the graphite crystals did not reflect enough light to be counted as empty space in the binary image.

The comparison of resistivity using raw NGPs and ultrasonically processed NGPs showed a general trend of decreased in resistivity. When the NGPs were sonicated for 2.0 minutes and added at a 8.0wt% loading, there was a decrease in resistivity of 0.5 Ωm. The small decrease in resistivity would suggest that breaking up the NGP agglomerations has a beneficial impact on the resistivity of the composite.

The comparison of mixing methods showed a decrease in resistivity when using the solution mixing instead of the melt mixing method. Decreases in resistivity suggests that there is

an increase in dispersion of the NGP particles. The increase in dispersion is also supported by the XRD characterization results. XRD spectra of the composite shows a peak positon shift for the semi-crystalline polymer. The peak shift to lower 2Θ values means that the d spacing between layers is increasing in the presence of NGP particles.

4.2. Electrical Properties

The shape of an I-V curve can be used to determine the type of electrical properties in a material. All of the I-V curves generated for the polymer composites indicates a non-linear relation between the current and resulting measured voltage. The non-linear shape shows that the material has semiconducting properties. Some of the semi-conducting properties could have come from non-ohmic contact creating the formation of a Schottky barrier diode. A Schottky barrier diode occurs at the junction of a metal (the tungsten probes) and an n-type semiconductor (graphene with electron charge transport). The possibility of non-ohmic contacts was not studied but would be an important characteristic to understand when the composites are integrated with a device.

4.3. Optimized Polymer composite for Melt Electrospinning

Electrical measurements preformed on the bulk composite for the optimized 6.0 wt% particle loading showed that the resistivity was dependent of the sonication time. Large agglomerations found in the samples, with no sonication, allowed the electrical charge to flow with the least resistance, shown by the steepest slope on the I-V curve and the lowest calculated resistivity. The large particles have very few junctions connecting to other particles. Junction areas are filled with an insulating polymer and would most likely have a resistance associated to each conductive particle junction. As the sonication time increased up to 3 minutes the resistivity of the composite decreased. At 4 minutes of sonication the resistivity increased back to a value

similar to the 2 minutes of sonication. The optimal sonication time of 3 minutes was most likely caused by the orientation of the particle packing. Ultrasonic energy breaks apart enough agglomerations to provide efficient packing of particles amongst the larger graphite crystals while keeping a lower number of junctions between particles. As the sonication time increased, a larger number of small particles were created which causes a significant increase in the number of junctions between each conductive particle.

After the composite material was electrospun the resistivity of fibers changed by an order of magnitude. The bulk polymer composite made from 6.0 wt% particle loading and 3 minutes of sonication had a resistivity of 200 Ω·m at 5.0 volts. After electrospinning, the same material had a new resistivity of approximately 20 Ω·m at 5.0 volts. The change in resistivity could be caused by an interaction between the conductive particles and the strong electric field created while electrospinning. Also, the resistivity of the composite fibers still had a dependence on sonication time but there was no longer an optimal time. The longer sonication times produced lower resistivities but all of the fiber resistivites began to converge to a constant resistivity of 6.0 Ω·m at approximately 80.0 volts.

5. Recommendations

Further research for this project should include additional material characterization, attempts to reduce the fiber diameter, and integrating the composite materials with previous research on fiber deposition control.

Additional material characterization techniques that were not used in this project would include Raman spectroscopy, rheology, and differential scanning calorimetry. Other research has shown that Raman spectra can be used to determine the number of graphene layers in multilayer graphene [33]. Detailed rheology data would help to understand the variation in viscosity as a function of shear rate and shear stress. Capillary rheology was demonstrated with the current configuration of the melt electrospinning tool but there was not enough data to present in this research [34]. Differential scanning calorimetry would be useful for determining a more accurate melting point of the composite and could show how the addition of dopants effects the melting point.

The original goal of the project was to produce fibers with a diameter on the order of 10 microns. During this project that goal was not achieved because of the high viscosity of the composite and the discontinuous fibers created during electrospinning. Electrospinning a conductive polymer composite is a complex system and could benefit from detailed research into the fundamentals, which could help solve the issue of discontinuous fiber deposition. The issue of discontinuous fiber deposition should be solved before trying to control the placement of the electrospun fibers.

6. References Cited

[1] Pinto N, Johnson Jr A, MacDiarmid A, Mueller C, Theofylaktos N, Robinson D, et al. Electrospun polyaniline/polyethylene oxide nanofiber field-effect transistor. Appl Phys Lett 2003;83(20):4244-4246.

[2] Ramasubramaniam R, Chen J, Liu H. Homogeneous carbon nanotube/polymer composites for electrical applications. Appl Phys Lett 2003;83(14):2928-2930.

[3] Naebe M, Lin T, Wang X. Carbon nanotubes reinforced electrospun polymer nanofibres. : InTech; 2010.

[4] Cadek M, Coleman J, Barron V, Hedicke K, Blau W. Morphological and mechanical properties of carbon-nanotube-reinforced semicrystalline and amorphous polymer composites. Appl Phys Lett 2002;81(27):5123-5125.

[5] Gao M, Dai L, Wallace GG. Biosensors based on aligned carbon nanotubes coated with inherently conducting polymers. Electroanalysis 2003;15(13):1089-1094.

[6] Nambiar S, Yeow JT. Conductive polymer-based sensors for biomedical applications. Biosensors and Bioelectronics 2011;26(5):1825-1832.

[7] Yang Y, Yu G, Cha JJ, Wu H, Vosgueritchian M, Yao Y, et al. Improving the performance of lithium–sulfur batteries by conductive polymer coating. Acs Nano 2011;5(11):9187-9193.

[8] Norton CL. Method of and apparatus for producing fibrous or filamentary material 1936.

[9] Lyons J, Li C, Ko F. Melt-electrospinning part I: processing parameters and geometric properties. Polymer 2004;45(22):7597-7603.

[10] Zhou H, Green TB, Joo YL. The thermal effects on electrospinning of polylactic acid melts. Polymer 2006;47(21):7497-7505.

[11] Callister WD, Rethwisch DG. Materials science and engineering: an introduction. : Wiley New York; 2007.

[12] Steric Arrangement In Polymers (Tacticity). 2015; Available at: http://polymerdatabase.com/polymer%20physics/Tacticity.html. Accessed July, 2016.

[13] Demirel B, Yaras A, Elcicek H. Crystallization behavior of PET materials. Journal of Journal of Bau Fen Bil.Enst.Dergisi Cilt 2011;13:26-35.

[14] Mark JE. Polymer data handbook. : Oxford university press; 2009.

[15] Chiang CK, Fincher Jr C, Park YW, Heeger AJ, Shirakawa H, Louis EJ, et al. Electrical conductivity in doped polyacetylene. Phys Rev Lett 1977;39(17):1098.

[16] Kalaitzidou K, Fukushima H, Drzal LT. A new compounding method for exfoliated graphite–polypropylene nanocomposites with enhanced flexural properties and lower percolation threshold. Composites Sci Technol 2007;67(10):2045-2051.

[17] Potts JR, Dreyer DR, Bielawski CW, Ruoff RS. Graphene-based polymer nanocomposites. Polymer 2011;52(1):5-25.

[18] Song P, Cao Z, Cai Y, Zhao L, Fang Z, Fu S. Fabrication of exfoliated graphene-based polypropylene nanocomposites with enhanced mechanical and thermal properties. Polymer 2011;52(18):4001-4010.

[19] Novoselov KS, Geim AK, Morozov SV, Jiang D, Zhang Y, Dubonos SV, et al. Electric field effect in atomically thin carbon films. Science 2004 Oct 22;306(5696):666-669.

[20] Novoselov K, Morozov S, Mohinddin T, Ponomarenko L, Elias D, Yang R, et al. Electronic properties of graphene. physica status solidi (b) 2007;244(11):4106-4111.

[21] Neto AC, Guinea F, Peres NM, Novoselov KS, Geim AK. The electronic properties of graphene. Reviews of modern physics 2009;81(1):109.

[22] Chung D. Exfoliation of graphite. J Mater Sci 1987;22(12):4190-4198.

[23] Cresti A, Nemec N, Biel B, Niebler G, Triozon F, Cuniberti G, et al. Charge transport in disordered graphene-based low dimensional materials. Nano Research 2008;1(5):361-394.

[24] Shen J, Chen X, Huang W. Structure and electrical properties of grafted polypropylene/graphite nanocomposites prepared by solution intercalation. J Appl Polym Sci 2003;88(7):1864-1869.

[25] Haggenmueller R, Gommans H, Rinzler A, Fischer JE, Winey K. Aligned single-wall carbon nanotubes in composites by melt processing methods. Chemical physics letters 2000;330(3):219-225.

[26] Bao Q, Loh KP. Graphene photonics, plasmonics, and broadband optoelectronic devices. ACS nano 2012;6(5):3677-3694.

[27] Pang H, Chen T, Zhang G, Zeng B, Li Z. An electrically conducting polymer/graphene composite with a very low percolation threshold. Mater Lett 2010;64(20):2226-2229.

[28] Leng Y. Materials characterization: introduction to microscopic and spectroscopic methods. : John Wiley & Sons; 2009.

[29] Wang M, Yan C, Ma L. Graphene nanocomposites. : InTech; 2012.

[30] Schroder DK. Semiconductor material and device characterization. : John Wiley & Sons; 2006.

[31] van der PAUYV L. A method of measuring specific resistivity and Hall effect of discs of arbitrary shape. Philips Res.Rep. 1958;13:1-9.

[32] Blackadder D, Le Poidevin G. Dissolution of polypropylene in organic solvents: 1. Partial dissolution. Polymer 1976;17(5):387-394.

[33] Ferrari AC, Basko DM. Raman spectroscopy as a versatile tool for studying the properties of graphene. Nature nanotechnology 2013;8(4):235-246.

[34] Whelan T, Dunning D. The Dynisco Extrusion Processors Handbook. : Dynisco Incorporated; 1988.

Appendix A: MATLAB Scrips

MATLAB scrips for averaging and comparing multiple data sets of I-V data taken with the four-point probe.

```
%   For the use in averaging data from several sequential files that have data arranged in the same format.
%   JDB
clear all; close all; clc;
color = {'b-','g:','r-.','c--','m-','k:'};
mult = inputdlg('How many data sets would you like to compare?','Compare Multiple Data Sets');
mult = str2num(mult{1});
if mult <= 0
   h = errordlg('REALLY!?! WTF Dude? You think that you can really compare less than 1 data sets? Two data sets is
a real comparison, I am just being nice letting you "compare" 1. Open MATLAB again and try this over!');
   uiwait(h);
   quit;
else
   seq = questdlg('Are the files numbered sequentially?','Query','Yes','No','Yes');
   if strcmp(seq,'No')
      errmsg = sprintf('The files that are to be averaged need to be sequential.\nPlease give your files sequentially
numbered names and try again.');
      errordlg(errmsg,'Error Reading Files');
   else
      for mindx = 1:1:mult
         clear volts;
         clear amps;
         infoprmt = {'Please enter the file name upto the first digit. Example: If your file is named NewFile_1.csv
enter NewFile_.','What is the first number of the sequence?','What is the last number of the sequence?','What is
the file extension (csv or xls)?'};
         infoDefaults = {'','1','5','csv'};
         info = inputdlg(infoprmt,'File Information',1,infoDefaults);
         frstnum = str2num(info{2});
         lastnum = str2num(info{3});
         flnm = info{1};
         extn = info{4};
         file = sprintf('%s%d.%s',flnm,frstnum,extn);
         if exist(file) == 0
            errordlg('This file cannot be found, please move this program to the same folder as the files.','Error');
         end
         legendTxt{1}=sprintf('Average %s',flnm);
         for ndx = frstnum:1:lastnum
            fulfile = sprintf('%s%d.%s',flnm,ndx,extn);
            legendTxt{ndx+1} = sprintf('%s%d',flnm,ndx);
            [data, text] =xlsread(fulfile);
            andx = strcmpi(text(7,:),'Value');
            vndx = strcmpi(text(7,:),'Reading');
            volts(ndx,:) = data(8:end,vndx)';
            amps(ndx,:) = data(8:end,andx)';
         end
         ampsAvg = zeros(1,length(amps(1,:)));
         voltsAvg = zeros(1,length(volts(1,:)));
         for inx = 1:length(volts(1,:))
```

```
            ampsAvg(1,inx) = mean(amps(1:ndx,inx));
            voltsAvg(1,inx) = mean(volts(1:ndx,inx));
        end
        titleTxt = sprintf('IV curve for the %s materials',flnm);
        figure(mindx);
        grid on;
        hold on;
        plot(voltsAvg,ampsAvg,'k','LineWidth',4);
        plot(volts',amps','LineWidth',2);
        legend(legendTxt,'Orientation','horizontal','Location','SouthOutside');
        ylabel('Current Injected (Amps)');
        xlabel('Voltage Reading (Volts)');
        title(titleTxt);
        hold off;
        avgLegend{mindx} = legendTxt{1};
        figure(mult+1);
        hold on;
        grid on;
        cindx = mindx-6*floor((mindx-1)/6);
        plot(voltsAvg,ampsAvg,color{cindx},'LineWidth',6);
        %title('Average IV for selected data sets');
        xlabel('Voltage Reading (Volts)');
        ylabel('Current Injected (Amps)');
        legend(avgLegend,'Location','SouthEast');
        hold off;
        resist = {'What is the probe spacing (meters)?','What is the total thickness of the sample, including the slide
(inches)','What is the slide thickness (mm)?'};
        resDefault = {'.001','','1'};
        res = inputdlg(resist,'Resistivity Calculations',1,resDefault);
        Gtyp = questdlg('Is the substrate conductive (G6) or non-conductive (G7)?','Conductivity','G6','G7','G7');
        rho0 = voltsAvg./ampsAvg*2*pi*str2num(res{1});
        w = str2num(res{2})*25.4-str2num(res{3});
        s = str2num(res{1})*1000;
        G7 = (2*s/w)*log(2);
        ws = w/s;
        if strcmp(Gtyp,'G7')
            if 0.1 <= G7 && G7 <= 10
                wrn = sprintf('The calculated value of G7(w/s) is: %f\nThe calcualted value of w/s is: %f\nDo these
values appear correct?',G7,ws);
                G7wrn = questdlg(wrn,'G7 Check','Yes','No','Yes');
                if strcmp(G7wrn,'No')
                    G7chs = questdlg('Would you like to use the calculated value or the look-up table?','Choose
Wisely','Calculated','Look-up','Calculated');
                    if strcmp(G7chs,'Look-up')
                        G7lookup = inputdlg('Please input the value of G7 from the look-up table:','G7 Look up');
                        G7 = str2num(G7lookup{1});
                    end
                end
            else
                bndWrndlg = sprintf('The value of G7 (%f) is outside the bounds of .1<G7<10. Would you still like to use
the calculated value?',G7);
                bndWrn = questdlg(bndWrndlg,'Out of Bounds','Yes','No','Yes');
                if strcmp(bndWrn,'No')
```

```
                G7lookup = inputdlg('Please input the value of G7 from the look-up table:','G7 Look up');
                G7 = str2num(G7lookup{1});
              end
            end
            G = G7;
          else
            G6lookup = sprintf('The value of (w/s) is: %f\nPlease enter the look-up value of G6:',ws);
            G6 = inputdlg(G6lookup,'G6 Look-up');
            G = str2num(G6{1});
          end
          legendRes{mindx} = sprintf('Average %s',flnm);
          rho = rho0./G;
          figure(mult+2);
          hold on;
          grid on;
          voltsPOS = find(voltsAvg >=0.5);
          plot(voltsAvg(voltsPOS), rho0(voltsPOS),color{cindx},'LineWidth',6);
          %plot(voltsAvg,rho,color{cindx});
          %title('Average resistivity of polymer after correction factor');
          ylabel('Resistivity (ohm-meters)');
          xlabel('Voltage (volts)');
          legend(legendRes,'Location','NorthEast');
          xlswrite('AvgRes.xlsx',rho',mindx);
        end
      end
    end
```

Appendix B: MATLAB Scrips

MATLAB scrips for averaging and comparing multiple data sets of I-V data taken with the van der Pauw method.

```
%   For the use in averaging data from several sequential files that have data arranged in the same
format.
%   JDB
clear all; close all; clc;
color = {'b','g','r','c','m','k'};
mult = inputdlg('How many data sets would you like to compare?','Compare Multiple Data Sets');
mult = str2num(mult{1});
if mult <= 0
   h = errordlg('REALLY!?! WTF Dude? You think that you can really compare less than 1 data sets? Two
data sets is a real comparison, I am just being nice letting you "compare" 1. Open MATLAB again and try
this over!');
   uiwait(h);
   quit;
else
   seq = questdlg('Are the files numbered sequentially?','Query','Yes','No','Yes');
   if strcmp(seq,'No')
      errmsg = sprintf('The files that are to be averaged need to be sequential.\nPlease give your files
sequentially numbered names and try again.');
      errordlg(errmsg,'Error Reading Files');
   else
      for mindx = 1:1:mult
         clear volts;
         clear amps;
         infoprmt = {'Please enter the file name upto the first digit. Example: If your file is named
NewFile_1.csv enter NewFile_.','What is the first number of the sequence?','What is the last number of
the sequence?','What is the file extension (csv or xls)?'};
         infoDefaults = {'','1','4','csv'};
         info = inputdlg(infoprmt,'File Information',1,infoDefaults);
         frstnum = str2num(info{2});
         lastnum = str2num(info{3});
         flnm = info{1};
         extn = info{4};
         file = sprintf('%s%d.%s',flnm,frstnum,extn);
         if exist(file) == 0
            errordlg('This file cannot be found, please move this program to the same folder as the
files.','Error');
         end
         legendTxt{1}=sprintf('Average %s',flnm);
         for ndx = frstnum:1:lastnum
            fulfile = sprintf('%s%d.%s',flnm,ndx,extn);
            legendTxt{ndx+1} = sprintf('%s%d',flnm,ndx);
            [data, text] =xlsread(fulfile);
```

```
        andx = strcmpi(text(7,:),'Value');
        vndx = strcmpi(text(7,:),'Reading');
        volts(ndx,:) = data(8:end,vndx)';
        amps(ndx,:) = data(8:end,andx)';
    end
    ampsAvg = zeros(1,length(amps(1,:)));
    voltsAvg = zeros(1,length(volts(1,:)));
    for inx = 1:length(volts(1,:))
        ampsAvg(1,inx) = mean(amps(1:ndx,inx));
        voltsAvg(1,inx) = mean(volts(1:ndx,inx));
    end

    titleTxt = sprintf('IV curve for the %s materials',flnm);
    figure(mindx);
    grid on;
    hold on;
    plot(voltsAvg,ampsAvg,'k','LineWidth',4);
    plot(volts',amps','LineWidth',2);
    legend(legendTxt,'Orientation','horizontal','Location','SouthOutside');
    ylabel('Current Injected (Amps)');
    xlabel('Voltage Reading (Volts)');
    title(titleTxt);
    hold off;
    avgLegend{mindx} = legendTxt{1};
    figure(mult+1);
    hold on;
    grid on;
    cindx = mindx-6*floor((mindx-1)/6);
    plot(voltsAvg,ampsAvg,color{cindx});
    title('Average IV for selected data sets');
    xlabel('Voltage Reading (Volts)');
    ylabel('Current Injected (Amps)');
    legend(avgLegend,'Orientation','horizontal','Location','SouthOutside');
    hold off;

    resist = {'What is the total thickness of the sample, including the slide (inches)','What is the slide
thickness (mm)?'};
    resDefault = {'','1'};
    res = inputdlg(resist,'Resistivity Calculations',1,resDefault);
    %Gtyp = questdlg('Is the substrate conductive (G6) or non-conductive
(G7)?','Conductivity','G6','G7','G7');

    w = (str2num(res{1})*25.4-str2num(res{2}))/1000;
    rho0 = 4.5323*w*(voltsAvg./ampsAvg);

    legendRes{mindx} = sprintf('Average %s',flnm);
    rho = rho0;
    figure(mult+2);
```

```
        hold on;
        grid on;
        plot(voltsAvg,rho,color{cindx});
        title('Average resistivity of polymer after correction factor');
        ylabel('Resistivity (ohm-meters)');
        xlabel('Voltage');
        legend(legendRes,'Orientation','horizontal','Location','SouthOutside');
        xlswrite('AvgRes.xlsx',rho',mindx);
      end
    end
end
```

Appendix C: MATLAB Scrips

MATLAB scrips for averaging and comparing multiple data sets of I-V data taken with the four-point probe on a fiber.

```
%   For the use in averaging data from several sequential files that have data arranged in the same
format.
%   JDB
clear all; close all; clc;
color = {'b-','g:','r-.','c--','m-','k:'};
mult = inputdlg('How many data sets would you like to compare?','Compare Multiple Data Sets');
mult = str2num(mult{1});
if mult <= 0
   h = errordlg('REALLY!?! WTF Dude? You think that you can really compare less than 1 data sets? Two
data sets is a real comparison, I am just being nice letting you "compare" 1. Open MATLAB again and try
this over!');
   uiwait(h);
   quit;
else
   seq = questdlg('Are the files numbered sequentially?','Query','Yes','No','Yes');
   if strcmp(seq,'No')
      errmsg = sprintf('The files that are to be averaged need to be sequential.\nPlease give your files
sequentially numbered names and try again.');
      errordlg(errmsg,'Error Reading Files');
   else
      for mindx = 1:1:mult
         clear volts;
         clear amps;
         infoprmt = {'Please enter the file name upto the first digit. Example: If your file is named
NewFile_1.csv enter NewFile_.','What is the first number of the sequence?','What is the last number of
the sequence?','What is the file extension (csv or xls)?'};
         infoDefaults = {'','1','5','csv'};
         info = inputdlg(infoprmt,'File Information',1,infoDefaults);
         frstnum = str2num(info{2});
         lastnum = str2num(info{3});
         flnm = info{1};
         extn = info{4};
         file = sprintf('%s%d.%s',flnm,frstnum,extn);
         if exist(file) == 0
            errordlg('This file cannot be found, please move this program to the same folder as the
files.','Error');
         end
         legendTxt{1}=sprintf('Average %s',flnm);
         for ndx = frstnum:1:lastnum
            fulfile = sprintf('%s%d.%s',flnm,ndx,extn);
            legendTxt{ndx+1} = sprintf('%s%d',flnm,ndx);
            [data, text] =xlsread(fulfile);
            andx = strcmpi(text(7,:),'Value');
```

```
            vndx = strcmpi(text(7,:),'Reading');
            volts(ndx,:) = data(8:end,vndx)';
            amps(ndx,:) = data(8:end,andx)';
        end
        ampsAvg = zeros(1,length(amps(1,:)));
        voltsAvg = zeros(1,length(volts(1,:)));
        for inx = 1:length(volts(1,:))
            ampsAvg(1,inx) = mean(amps(1:ndx,inx));
            voltsAvg(1,inx) = mean(volts(1:ndx,inx));
        end
        titleTxt = sprintf('IV curve for the %s materials',flnm);
        figure(mindx);
        grid on;
        hold on;
        plot(voltsAvg,ampsAvg,'k','LineWidth',6);
        plot(volts',amps','LineWidth',6);
        legend(legendTxt,'Location','SouthEast');
        ylabel('Current Injected (Amps)');
        xlabel('Voltage Reading (Volts)');
        %title(titleTxt);
        hold off;
        avgLegend{mindx} = legendTxt{1};
        figure(mult+1);
        hold on;
        grid on;
        cindx = mindx-6*floor((mindx-1)/6);
        plot(voltsAvg,ampsAvg,color{cindx},'LineWidth',6);
        %title('Average IV for selected data sets');
        xlabel('Voltage Reading (Volts)');
        ylabel('Current Injected (Amps)');
        legend(avgLegend,'Location','SouthEast');
        hold off;
        resist = {'What is the probe spacing (m)?','What is the total diameter of the fiber? (m)'};
        resDefault = {'0.001',''};
        res = inputdlg(resist,'Resistivity Calculations',1,resDefault);
        %Gtyp = questdlg('Is the substrate conductive (F12) or non-conductive
(F11)?','Conductivity','F12','F11','F11');
        D = str2num(res{2});
        s = str2num(res{1});
        rho0 = ((voltsAvg./ampsAvg)*((3.14/4)*D^2))/(s);

        legendRes{mindx} = sprintf('Average %s',flnm);
        %rho = rho0*F11*F2*F32;
        figure(mult+2);
        hold on;
        grid on;
        voltsPOS = find(voltsAvg >=0.5);
        plot(voltsAvg(voltsPOS), rho0(voltsPOS),color{cindx},'LineWidth',6);
```

```
        ylabel('Resistivity (ohm-meters)');
        xlabel('Voltage (volts)');
        legend(legendRes,'Location','NorthEast');
        xlswrite('AvgRes.xlsx',rho0',mindx);
      end
    end
end
```

SIGNATURE PAGE

This is to certify that the thesis prepared by Brandon Ross entitled "Fabrication and Characterization of Conductive Melt Electrospun Fibers" has been examined and approved for acceptance by the Department of General Engineering, Montana Tech of The University of Montana, on this 3th day of August, 2016.

Jack L. Skinner, Ph.D., Associate Professor
Department of General Engineering
Chair, Examination Committee

Brahmananda Pramanik, Ph.D. Assistant Professor
Department of General Engineering,
Member, Examination Committee

Katie Hailer, Ph.D., Associate Professor
Department of Chemistry
Member, Examination Committee